Bioactive Materials 6 (2021) 2198–2220

Contents lists available at ScienceDirect

Bioactive Materials

journal homepage: www.sciencedirect.com/journal/bioactive-materials

Cardiac mechanostructure: Using mechanics and anisotropy as inspiration for developing epicardial therapies in treating myocardial infarction

Kiera D. Dwyer, Kareen L.K. Coulombe *

Center for Biomedical Engineering, School of Engineering, Brown University, Providence, RI, USA

ARTICLE INFO

Keywords:
Anisotropy
Cardiac biomechanics
Epicardial therapies
Ventricular restraint
Cardiac tissue engineering

ABSTRACT

The mechanical environment and anisotropic structure of the heart modulate cardiac function at the cellular, tissue and organ levels. During myocardial infarction (MI) and subsequent healing, however, this landscape changes significantly. In order to engineer cardiac biomaterials with the appropriate properties to enhance function after MI, the changes in the myocardium induced by MI must be clearly identified. In this review, we focus on the mechanical and structural properties of the healthy and infarcted myocardium in order to gain insight about the environment in which biomaterial-based cardiac therapies are expected to perform and the functional deficiencies caused by MI that the therapy must address. From this understanding, we discuss epicardial therapies for MI inspired by the mechanics and anisotropy of the heart focusing on passive devices, which feature a biomaterials approach, and active devices, which feature robotic and cellular components. Through this review, a detailed analysis is provided in order to inspire further development and translation of epicardial therapies for MI.

1. Introduction

In the United States alone, approximately 720,000 people will suffer from a myocardial infarction (MI) each year [3]. MI occurs when blood flow to the myocardium is obstructed, resulting in myocardial ischemia and cardiomyocyte death. Acute MI treatments focus on reperfusion therapies that restore blood flow in order to preserve cardiomyocyte survival and limit ischemic injury. Reperfusion is not always enough to preserve cardiac function, however. Reduced systolic function post-MI can trigger pathological ventricular remodeling to compensate for reduced cardiac output. If left untreated, or if a patient is not responsive to maximal drug therapy, this remodeling can lead to heart failure (HF). With an estimated 30% of patients surviving MI further developing HF and the gold standard treatment being heart transplantation, improved therapies post-MI must be developed [4].

In an attempt to enhance MI treatment and limit its progression to HF, a new class of cardiac therapies have emerged: epicardial restraint devices. These biomaterial-based devices are implanted on the infarcted region of the myocardium and work to mechanically reinforce the ventricular wall in order to prevent pathological remodeling and thus improve cardiac function. Advancements in tuning the mechanical and structural properties of these materials have greatly contributed to their ability in providing appropriate restraint. Recent pre-clinical improvements to such therapies feature composite systems with robotic or cellular components, which directly compensate for the loss of contracting cardiomyocytes in the ischemic myocardial regions.

Success in translating new technologies largely relies on our understanding of the changes induced in the myocardium post-MI. Therefore, in this review, the mechanical and structural properties of the healthy and infarcted myocardium will be investigated. Through identification of the environment in which the therapy must perform as well as the functional deficiencies induced by MI which the therapy must address, necessary properties of the biomaterial-based cardiac therapies will be determined. Then, the epicardial devices, as well as the engineering techniques used to fabricate them, will be explored as potential therapies. Epicardial therapies will be discussed in two categories: passive devices, which feature a biomaterials approach, and active devices, which feature robotic and cellular components, as illustrated in Fig. 1.

2. Cardiac Mechanostructure

When considering the movement of the heart, or “cardiac motion,”

Peer review under responsibility of KeAi Communications Co., Ltd.
* Corresponding author. School of Engineering, Brown University, 184 Hope Street, Box D, Providence, RI, 02912, USA.
E-mail address: kareen_coulombe@brown.edu (K.L.K. Coulombe).

https://doi.org/10.1016/j.bioactmat.2020.12.015
Received 30 September 2020; Received in revised form 18 December 2020; Accepted 18 December 2020

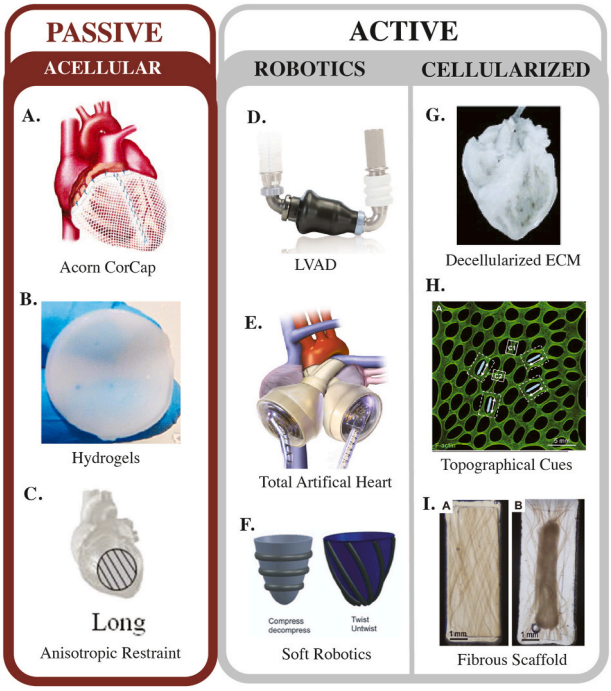

Fig. 1. Epicardial therapies for post-MI support. Passive restraint devices are acellular and may be homogeneous (i.e., non-directional and isotropic) to cover the whole heart, such as the Acorn CorCap (A), cover a local area such as hydrogels (B) or be anisotropic (C). Active cardiac support devices include mechanical circulatory support such as left ventricular assist devices (LVAD, D), total artificial heart (E) and novel robotics (F) or cellular implants (G–I). The structure and anisotropy of cellular engineered tissues may originate from decellularized native tissue (G), hydrogel molding techniques with topographical cues (H) or fibrous scaffolds where hydrogel and cell mixtures are cast upon fibers (I). (A) Reprinted from Ref. [1] with permission from Elsevier; (B) Reprinted with permission from Ref. [5], Copyright 2020 American Chemical Society; (C) Reprinted from Ref. [6] with permission from Elsevier; (D) HeartMate II is a trademark of Abbott or its related companies. Reproduced with permission of Abbott, © 2020. All rights reserved; (E) Reproduced with permission of SynCardia, © 2020. All rights reserved; (F) From Ref. [7]. Reprinted with permission from AAAS; (G) Reprinted from Ref. [8] with permission from Elsevier; (H) Reprinted from Ref. [9] with permission from Elsevier; (I) Reprinted from Ref. [2] with permission; the publisher for this copyrighted material is Mary Ann Liebert, Inc. publishers.

an immediate appreciation emerges for its continuous, coordinated and dynamic nature. During the cardiac cycle, the heart undergoes synchronized contraction and subsequent deformation to create torsion, a motion comparable to the wringing out a wet towel. This unique motion optimizes the volume of blood pumped from the left ventricle thus ensuring sufficient circulation of oxygenated blood to the body.

Contraction of the heart is largely dependent on two key factors: **(1) mechanical environment** and **(2) anisotropic structure**. Even more important is the cooperation between these two factors. For example, during a healthy cardiac cycle, the myocardium contracts to shorten between 15 and 20% and develops a peak stress of 22 mN/mm^2 [10]. If myocardial mechanics was the only determinant of cardiac function, the ejection fraction of the heart would be significantly less than the physiological ejection fraction of >50% [11–13]. Sallin et al. demonstrated through mathematical modeling of the heart as an ellipsoid with myocardial fibers oriented sole in the circumferential direction could yield an ejection fraction of only 30%; however, when helical fiber organization was considered, a physiological-relevant ejection fraction of 60% could be achieved [14]. Such modeling illustrates the importance of myocardial fiber organization within the ventricle wall and further its ability to ensure efficient cardiac pumping.[1]

A major step in studying cardiac motion, and moreover the relationship between cardiac mechanics and structure, arises from advancements in imaging technologies. Such technologies, some of which are outlined in Table 1, have enabled researchers to study the cardiac cycle *in vivo*. Inherently noninvasive techniques such as echocardiography, magnetic resonance imaging (MRI) and computed tomography (CT) have been widely used in clinical practice to investigate global cardiac structure and function [11,15]. Although these imaging modalities are insightful, they do not capture the mechanical function of the heart at a local level. Recently, techniques to quantify local mechanics, such as strain profiles, degree of rotation and angular velocity within the ventricular wall, have proven to be sensitive indices in detecting ventricular performance [16]. These metrics can be measured by tracking myocardial motion non-invasively through speckle tracking echocardiography [17,18], tagged-MRI [19], 4D ultrasound with 3D strain mapping [20] as well as tracking transmural myocardial fiber organization through diffusion tensor MRI [21–23] and 3D ultrasound backscatter tensor imaging [24]. These techniques are especially important when considering cardiovascular diseases such as heart failure with preserved ejection fraction (HFpEF), recently declared by the National Heart, Lung and Blood Institute as the "greatest unmet need in cardiovascular medicine" [25]. In HFpEF, the ejection fraction of the heart remains within a physiologically healthy range while the left ventricle experiences diastolic dysfunction. By utilizing more sensitive metrics of local ventricular function, better detection, such as in the case of HFpEF, and mechanistic understanding of cardiovascular diseases can be achieved.

Through these advancements it is clear that cardiac *mechanics* – how the myocardium responds to force- and *structure* – which dictates the functional implications of the mechanics-play key roles in proper cardiac function.

2.1. Cardiac biomechanics

Throughout the cardiac cycle, different forces act upon and within the myocardium, with the average diastolic tension and peak developed stress in humans reaching 11 mN/mm^2 and 22 mN/mm^2, respectively [10]. The biomechanical function of the heart can be easily visualized as a pressure-volume (PV) loop, a graph which relates ventricular volume (x-axis) with pressure (y-axis) during a cardiac cycle. One key metric is stroke volume (SV), defined as the volume of blood ejected during contraction of the ventricle. SV is calculated as the difference between the end systolic volume (ESV) and end diastolic volume (EDV).

The mechanical environment of the myocardium, specifically the pre- and after-loading conditions, can significantly impact SV. Preload refers to the initial force placed on the ventricle which occurs during diastolic filling to induce cardiomyocyte stretching. Factors such as venous return, diastolic wall stiffness, filling time and atrial stiffness significantly impact the force of preload [26]. Afterload, on the other hand, refers to the force the heart must contract against and is largely determined by factors such as arterial pressure, arterial resistance and aortic valve function [26]. Abnormal preload and afterload conditions have been associated with ventricular dysfunction. Structurally, sarcomeres within the cardiomyocyte rearrange in response to abnormal loading conditions in order to preserve cardiac output. Increased preload (known as volume overload) and afterload (known as pressure

[1] Estimates are adapted from Ref. [7]. For an ellipsoid hemisphere with a height of H, radius of R and uniform shortening of the fibers to k times their initial length, the initial volume (V_i) and final volume (V_f) would be: $V_i = \frac{2}{3}\pi HR^2$ and $V_f = V_i = \frac{2}{3}\pi HR^2k^2$. Ejection fraction is calculated by: $EF = \frac{V_f - V_i}{V_i}$. Using the volume equations for an ellipsoid hemisphere, the ejection fraction can be solved for 1-k^2. This equation illustrates that a large ejection fraction cannot be obtained through physiologically shortening. For example, at 20% fiber shortening (k = 0.8) the ejection fraction corresponds to 0.36.

Table 1
Measuring functional mechanics and anisotropy in the heart.

	Technology	Description	Application
Global Structure and Function	Echocardiography	Uses sound waves; portable, noninvasive, fast; 2D or 3D	2D ventricular dimensions throughout the cardiac cycle, 3D end-systolic and end-diastolic volumes, wall thickness, structural abnormalities, ejection fraction, stroke volume, cardiac output
	Cardiac Magnetic Resonance Imaging (MRI)	Application of magnetic field; noninvasive; uses ECG gating; higher resolution compared to echocardiography; sensitive to motion artifact	2D ventricular dimensions throughout the cardiac cycle, 3D end-systolic and end-diastolic volumes, wall thickness, structural abnormalities, ejection fraction, stroke volume, cardiac output
	Computed tomography (CT)	Uses X-ray and often requires a contrast agent	3D images of the heart, visualization of vasculature
	Catheterization	Invasive	Pressure-volume measurements
Local Strain Profiles and Fiber Organization	Speckle tracking Echocardiography (STE)	Utilizes speckle pattern in myocardium	Location deformations, stress/strain, rotation and twisting
	Tagged Magnetic Resonance Imaging	Tracks altering of longitudinal magnetization	Location deformations, stress/strain, rotation and twisting
	4D Ultrasound with 3D Strain Mapping	Combines ultrasound imaging with post-imaging analysis	3D strain mapping
	Diffusion Tension Magnetic Resonance Imaging (DT-MRI)	Based on principle orientation of microstructure and diffusivity of water parallel; sensitive to motion artifact	Fiber orientation changes during the cardiac cycle
	3D Ultrasound Backscatter Tensor Imaging	Ultrafast ultrasound; quantify spatial coherence of backscattered echoes	Fiber orientation changes during the cardiac cycle
	Doppler tissue	Higher temporal resolution compared to MRI	Blood flow velocities, torsion angular velocity
	Gyroscopic sensors	Invasive	Twisting of different ventricular regions based on placement of sensors; angle of rotation and velocity

overload) induce eccentric and concentric hypertrophy, respectively. In the former case, sarcomeres respond to the increased diastolic stress and volume demand by assembling in series, which subsequently leads to chamber enlargement [27]. In the latter case, sarcomeres assemble in parallel in response to increased systolic stress, effectively increasing the thickness of the ventricular wall [27]. Both preload and afterload forces have also been shown to regulate the expression of fetal genes [28,29]. Toischer et al. differentiated between preload and afterload conditions, finding Akt activation without fibrosis and little apoptosis associated with the former and CaMKII-dependence, fibrosis and apoptosis associated with the latter [30].

The concept of preload and afterload are often utilized in engineering cardiac tissue. In its simplest form, these loads are introduced into the engineering of cardiac tissue through posts at the tissue ends, used to induce stretch (preload) as well as provide a flexible beam against which the tissue must contract against (afterload) [31]. More complicated systems feature mechanical bioreactors programed with dynamic cyclic loading sequences which control the length at which the tissue is stretched and/or the force applied against tissue contraction [32,33]. Increased afterload has been described to enhance the functional maturity of engineered cardiac tissue as evidenced by increased sarcomere alignment, cardiomyocyte elongation [33], tissue compaction and force of contraction [34] and improved calcium handling [33] as compared to controls without afterload. However, similar to *in vivo* observation, there is an optimal range for preload and afterload conditions *in vitro*. Hirt et al. found engineering cardiac tissue with posts reinforced with metal braces results in hypertrophic enlargement, activation of fetal genes, as well as reduced contractile force and diastolic relaxation even when the afterload is released [35].

2.1.1. Mechanical contribution of the elastin-rich epicardium

Unsurprisingly, much of research surrounding cardiac biomechanics focuses on the myocardium of the heart as this layer contains cardiomyocytes, the cells responsible for active contraction of the heart. However, the ventricular wall of the heart contains two more layers: the epicardium (outermost layer, inner layer of the serous visceral pericardium) and the endocardium (innermost layer), both of which are made up of elastin fibers embedded within a collagen network. The myocardial extracellular matrix (ECM) plays a key role in defining the overall helical architecture of the heart, promoting active contraction by the cardiomyocytes within its network and ensuring appropriate passive stretch to prevent overstretching during diastole. However, recent scientific discoveries have implicated the elastin-rich epicardial layer as another key component in regulating cardiac mechanics [36,37].

Elastin is an important component in soft tissues as it allows for long-range deformability, promotes passive recoil and efficiently stores and releases energy during dynamic loading. Although its role in cardiac biomechanics is still being elucidated, elastin has been well studied in arteries. At low pressures in arteries, most of the load is placed on elastin, allowing the artery to be compliant and stretch. At higher pressures, however, the load is transferred to the collagen fibers of the artery, which limit its dilation to prevent rupture [38]. Although artery compliance is tangentially related to cardiac mechanics, understanding the role of elastin and its relationship with collagen in the arteries, a well-studied system, gives insight into the potential importance and function of elastin in cardiac cyclic loading.

Recent studies have investigated the mechanical role of the epicardial layer [36,37]. The epicardial layer is under tension *in vivo*; removal of this load by explant results in the recoil of the epicardium and subsequent bending of the ventricular tissue attached to it. The bending angle of this recoil can be quantified at various anatomical regions of the heart in order to gain insight into the regional role of the epicardium in cardiac mechanics. One such study was performed by Shi et al., who not only extensively outlined the characterization of such bending angles but also provided valuable insights about the functional role of the elastin-rich epicardium. Shi et al. quantified epicardial pre-strain in different anatomical regions and orientations in the heart and used a finite element model to demonstrate that epicardial pre-strain modulated ventricular expansion during diastole [36]. Additionally, Jöbsis et al. studied the epicardium structure illustrating that parallel elastin rods run along collagen fibers at the surfaces of the epicardium but is independent of collagen orientation in the midsection [37]. When the epicardial region was removed by blunt dissection, Jöbsis et al. reported a decrease in the passive stiffness at lower ventricular volumes. These studies serve as an important and significant step in enhancing the understanding of the biomechanical mechanism of the heart beyond that of the myocardium and inspire further research into how such mechanics are impacted or even contribute to cardiovascular disease, such as MI and HF.

2.2. Cardiac anisotropy

The global organization of myocardial fibers explains the twisting motion and functional efficiency of the heart throughout the cardiac cycle. According to the Torrent-Guasp model, discerned through gross dissections, the ventricle consists of a helically organized myocardial band [39]. This band contains oblique, overlaying myocardial sheets with fiber angles rotating up to 104° from the endocardium (inner) to epicardium (outer) layer in the left ventricle of humans [40]. In the sub-endocardium region, fibers are organized longitudinally at an angle of approximately +40° relative to the circumferential axis of the heart, essentially creating a right-handed helical structure. Through the mid-wall of the ventricle fibers rotate in a counterclockwise manner, resulting in a largely circumferentially organization. At the epicardial wall, the fibers reach an angle of approximately −60° relative to the circumferential axis of the heart and resemble a left-handed helical structure [11,40]. A schematic of the helical organization of myocardial fibers is depicted in Fig. 2.

Based on this structural explanation – right-handed helical conformation conformation in the endocardium and left-handed helical conformation in the epicardial region – contraction in the endocardium results in the ventricular base rotating in the counterclockwise direction and the apex rotating in the clockwise direction. However, in the epicardial region of the ventricular wall, this directionality is reversed [11]. These motions do not cancel each other out, however, for two reasons: timing and torque. The timing of contraction is largely determined by the bundle of His, highly conductive fibers that form branches known as the Purkinje fibers that propagate the electrical signal to the ventricle. Based on the anatomically location of the Purkinje fibers, the endocardium is the first region in the left ventricle to be electromechanically activated [41]. This activation causes sub-endocardial shortening and sub-epicardial stretching, resulting in clockwise rotation at the apex and counterclockwise at the ventricular base. The electrical signal eventually reaches the epicardium. Because torque is proportional to the distance from the center of rotation, contraction of the sub-epicardial myocardial fibers dominates the overall cardiac rotational motion [42,43]. However, due to the opposing motion in the sub-endocardium region, a shear force develops toward the ventricle cavity, inducing fiber reconfiguration and wall thickening. Like a spring, these fiber store potential energy which is used in the recoil of the ventricle during isovolumetric relaxation [43].

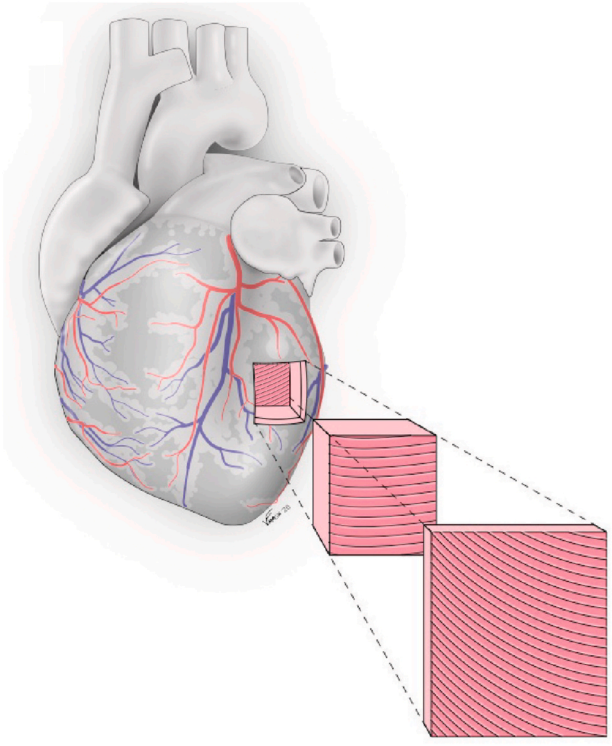

Fig. 2. Anisotropic structure of the heart. The myocardial fiber orientation varies transmurally throughout the ventricle wall in a left-handed helix at the endocardium and rotating through circumferential orientation mid-wall into a right-handed helix at the epicardium to contribute significantly to the efficiency in cardiac pumping. This fiber organization is disrupted by MI, contributing to reduced cardiac output.

The fiber angle gradient within the ventricular wall is responsible for the longitudinal and circumferential motion of cardiac torsion. Utilizing 2D speckle tracking echocardiography on human patients (ages 25–55), Zhang et al. measured peak apical and basal torsion to be around −5° and 13°, respectively and peak untwisting velocity to be around 100°/sec [44]. It should be noted, however, that these values vary significantly depending on age, likely due to the architectural changes of myocardial fiber during early development and late aging. Nagata et al. further investigated the strain gradient within the ventricular wall, calculating the global longitudinal strain in the endocardial, transmural, and epicardial regions of the left ventricle as −23.1%, −20.0% and −17.6% and circumferential strains in the same regions as −28.5%, −20.8% and −15.3% [45].

An important theme thus established in studying the structure of the heart is anisotropy, or directionally dependent properties. Although anisotropy is important at the global scale in order to induce torsion, this property also functions at the cellular level in tension generation and electrical signal propagation. Individual cardiomyocytes have a rod-like shape, featuring an aspect ratio of ~7:1 which allows for the establishment of a major axis within the cell [46]. In the myocardium, cardiomyocytes have approximately 11 neighbors in space, with cell-cell junctions occurring predominately in the longitudinal direction or through branching at acute angles [47]. Further, the size and shape of cardiomyocytes are significantly influenced by its extracellular environment. Using fibronectin, Bray et al. created patterns with varying aspect ratio upon which neonatal rat cardiomyocytes were cultured [46]. As the aspect ratio of the pattern increased, myofibrils and sarcomeres within the cardiomyocytes had improved longitudinal alignment, effectively demonstrating that geometric cues from the ECM play a significant role to reconfigure the intracellular architecture of cardiomyocytes.

The anisotropy of cardiomyocyte also influences its function. Because the sarcomeres are the contractile machinery of the cardiomyocyte, their alignment along a major axis and elongation close to the 2.2 μm length observed in adult cardiomyocytes allows unidirectional, forceful contraction as compared to randomly oriented sarcomeres [48]. Additionally, anisotropy influences propagation of electrical signals by promoting the polarization of extracellular gap junctions to the longitudinal ends of the cardiomyocytes. The anisotropic structure influences the size and shape of the intracellular cytoplasm, a medium which has low resistivity to electrical propagation, and polarization of the intercellular junction, a structure which has high resistivity to electrical signal propagation [49]. Thus, controlling cardiomyocyte anisotropy *in vitro* has resulted in changes to the conduction velocity and action potential duration of the cell [48,50].

The importance and functional impact of cardiac anisotropy varies based on the length scale of focus and the integration of all components, from cells to fibrous structure and macroscopic features. An advanced understanding of cardiac anisotropy can be leveraged to engineer biomaterials that advance cardiac function through recapitulation of the hierarchical, anisotropic structure of the heart.

2.3. Functional consequences of cardiac mechanostructure

Optimal cardiac function requires multiscale cooperation between the mechanical environment and anisotropic structure of the heart. The

unique properties of the myocardium in regard to these two factors have key functional consequences. It is in understanding these functional consequences – and investigating how MI changes them – that biomaterials for epicardial restraint therapies can be engineered with properties that are appropriate to improve cardiac function.

Frank Starling Law – The Frank Starling law, which is based on the length-tension relationship observed in striated muscle, relates diastolic volume with stroke volume in the heart [51]. Through this mechanism, increased stretching, such as that induced by increased diastolic volume, increases the force of contraction by the cardiomyocyte. It is important to note that there is a maximum limit to this relationship, an important factor in engineering materials with appropriate compliance.

Law of Laplace - The Law of Laplace states that wall stress within a spherical wall at a given pressure is inversely proportional to the wall thickness [52]. This is especially significant in considering ventricular stress and strain profiles during physiological or pathological ventricular remodeling, in which the thickness in the ventricular wall can change. In the case of myocardial infarction, for example, ventricular dilation, infarct thinning and even rupture are not uncommon. Accordingly, this thinning will increase the ventricular wall tension. Epicardial cardiac biomaterials mechanically reinforce areas of thinning and high tension; however, appropriate mechanical properties of these biomaterials must be closely considered.

Mechanics and anisotropy impact torsion– Loading conditions can directly impact the ability of the myocardium to generate torsion through changing the contractility of the cardiomyocytes. Increasing preload, according to the Frank Starling mechanism, increases contractility and peak rotational angle while afterload reduces both [43]. Disruption of anisotropy also impacts the ability of the heart to generate torsion. Cardiac fiber rearrangement associated with aging [44,53], pressure load hypertrophy [54], HF [55] and MI [22,23] lead to changes in torsion metrics. For example, during aging sub-endocardial fibers rearrange and become unable to counter the torque produced by the epicardial region. Functionally, this results in increased peak twist angle [44,53]. In MI, loss of fibers or disruption of their structure can be observed in the infarcted region [23]. Further, ventricular dilation can cause the myocardial fibers on the surfaces of the ventricle to orient circumferentially. The difference in fiber orientation between the endocardial and epicardial surfaces increases, challenging the delicate balance necessary for optimal torque generation [11,22].

3. The Response of Cardiac Mechanostructure to MI

During MI, cardiomyocytes, starved of oxygen and nutrients, progressively die downstream of an arterial occlusion until blood flow can be restored to the infarcted region or the oxygen tension is sufficient to curb cardiomyocyte necrosis. This myocardial death, and its subsequent healing, drastically changes the mechanical and structural landscape of heart.

When blood flow is restored to the infarcted region post-MI, a healing process is triggered with the goal of maintaining cardiac function. Often times, however, MI causes injury beyond the heart's intrinsic ability to repair itself. In developing new therapies for extrinsic repair, it is important to understand the mechanics and structure of the myocardium during this healing process because (1) these factors impact the severity of infarct damage, expansion and rupture, as well as its potential progression to HF [56]; and (2) these factors can impact the cardiac response to therapies, especially when exogeneous cells are introduced to the ischemic environment [57–60].

An extensive review by Holmes, Borg and Covell explores the structural and mechanical changes during the MI healing process [56]. In it Holmes et al. postulate that specific elements of the cardiac environment dominate the mechanics at different stages of infarct healing. They outline four phases: acute ischemia governed by the passive myocardium; necrotic phase governed by edema, fibrotic phase governed by the deposition of large collagen fibers; and the remodeling phase governed by collagen crosslinking. The focus of this review will be on advancements in understanding these phases which are vital in engineering *in vivo* therapies.

3.1. Acute ischemia: the passive myocardium

During the first 30 seconds of hypoxia following coronary occlusion, the myocardium loses its ability to generate active force, effectively acting as a passive, viscoelastic material [61]. The passive mechanical properties of the myocardium are largely determined by the tension developed intracellularly (cardiomyocytes) and extracellularly (collagen fibers). The tension level determines which of these components dominates. Granzier and Irving calculated that at low tension levels (sarcomere lengths between 1.9 and 2.1 μm), titin contributes 70% to the passive tension of cardiac rat muscle while at higher tensions (sarcomere lengths above 2.1 μm), the extracellular collagen contribution increased sharply to 80% [62].

At low tensions, the intracellular myofilament, titin, largely determines the passive properties of the myocardium. Spanning from the Z-disk to the M-band on the sarcomeres of individual cardiomyocytes, titin acts as a spring to prevent overextension of the sarcomeres along the myofilament axis. Mutations in titin are the leading cause of familial dilated cardiomyopathy, presumably due to the inability of the heart to create passive tension and thus prevent dilation upon force [63]. Post-translational phosphorylation [64,65], disulfide bridge formation [66], calcium binding [66–68] and different isoforms [69–71] can have a significant impact on the stiffness of titin and thus the myocardial environment. For example, the N2BA titin isoform has a longer extendable I-region, resulting in increased compliance, as opposed to its counterpart N2B [69]. The ratio of these isoforms thus determines the contribution of titin to the passive stiffness of the myocardium, with humans having a ratio of N2BA/N2B ~0.6 [70].

At higher tensions, collagen fibers dominate the mechanical properties of the passive myocardium. Collagen is composed of three left-helix polypeptide chains intertwined to form a triple helix structure. Under physiological condition, tropocollagen, which is defined as the collagen triple helix with its exposed amino and carboxy-prolylpeptide cleaved, self assembles into fibrils, which feature staggered gaps on the order of 60 nm. These fibrils form the commonly referenced collagen fibers [72]. Collagen fibers contain macroscopic crimps, based on the organization of the fibers, as well as nanoscale crimps, which are regions of the collagen helices deficient in the amino acid, hydroxyproline, a key compound involved in the hydrogen bonding responsible for maintaining the helical structure [73,74]. When strain is applied to the collagen fiber, these crimps straighten, resulting in a region with little stress development, known as a "toe region." With increasing stress, no further entropic extension is possible and a linear region on the stress-strain graph ensues, representing the response from the sliding of collagen fibrils and stretching of the triple helix [74].

3.2. Necrotic phase: degradation

Following the acute ischemia is a phase marked by inflammation, degradation and death. Within 24 hours, necrotic cardiomyocytes lose their striations [75] and a phenotype of "wavy fibers," most likely from stretching of fibers during systole, ensues [76]. This is indicative of the degradation of titin and collagen. There is also an imbalance between matrix metalloproteinases (MMPs), which degrade components of the ECM, and tissue inhibitors of metalloproteinases (TIMPs). This imbalance is evidenced by spatiotemporal peaks in MMP activation - specifically MMP-1 (collagenase), MMM-2 and MMP-9 (gelatinase) – which degrade the ECM environment [77–79]. The removal of necrotic cardiomyocytes coupled with the degradation of the ECM results in increased infarct compliance and expansion as cardiomyocytes slip past each other. Unsurprisingly, the highest risk of ventricular dilation and infarct rupture occurs during this phase [80]. This increased

compliance, however, quickly shifts to increased stiffness attributed to swelling as early as 4–6 h post-MI in large animal [56].

3.3. Fibrotic phase: deposition

After the necrosis stage of MI healing, new ECM is rapidly deposited in the infarcted area. This change in the ECM can significantly impact cellular function, as evidenced by Sewanan et al. Using decellularized ECM from porcine carrying a hypertrophic cardiomyopathy mutation, Sewanan demonstrated that the diseased ECM provokes abnormal behavior in the contractility of otherwise healthy cardiomyocytes [81]. The content, composition and organization of the new ECM thus plays a vital role in the infarct mechanics and further cardiomyocyte function.

3.3.1. Mechanical changes

After MI, the collagen content in the infarct region rapidly increases, which correlates with increased stiffness [56]. Barry et al. highlights this increase, measuring the elastic modulus to be 18 kPA in the healthy, remote rat myocardium, 55 kPa in the infarcted myocardium and changing at a rate of −8.5 kPa/mm (in the direction from the infarct toward the remote region) within the border region [82].

Although critical in preventing infarct rupture, increased collagen, and thus stiffness, can impact systolic contraction and limit diastolic stretching in the infarcted and/or adjacent regions. At the cellular level, *in vitro* testing has illustrated the impact of material properties, particularly stiffness, on cardiomyocyte spreading [60,83], contractility [57–60], sarcomere alignment [57,58], β-MHC expression [83] and calcium handling [58]. Ultimately, these studies indicate that optimal cardiomyocyte function occurs on substrate stiffnesses close to that of healthy myocardium (~10 kPa). In addition to these studies, researchers have developed systems and studied the mechanical environment of the myocardium post-MI. Corbin et al. developed a magnetorheological elastomer in which stiffness can be tuned instantaneously based on the distance between the substrate and magnet in order to more closely model the stiffness changes post-MI [83]. Additionally, Nguyen et al. utilized different substrate stiffnesses to mimic the healthy myocardium (~14 kPa) as well as the myocardium 1-week post-MI (~83 kPa) and 2–6 weeks post-MI (~484 kPa) to investigate the impact of substrate stiffness at the cardiomyocyte – cardiac fibroblast boundary. This study found the magnitude of the transmitted force and propagating distances over the boundary were inversely related to substrate stiffness [59].

3.3.2. Compositional changes

The content of collagen is not the only contributing factor to the change in the mechanical properties of the post-MI myocardium. The composition of the ECM deposited in the infarcted area varies significantly compared to that of healthy myocardium.

One week after MI in rat models, the extracellular protein periostin increases five-fold accompanied by slight increases in fibronectin and collagen VI and decreases in collagen I, collagen XV and laminin [84]. More dramatically is that by four weeks after MI, collagen I comprises of 57% of the extracellular proteins, as compared to 16% in healthy myocardium [84]. These compositional changes are important for both the structure and signaling functions of the ECM. For example, periostin, which is typically only found in healthy myocardium at early embryogenesis stages, is abundant in the infarct border zone [85]. Periostin has been found to regulate collagen 1 fibrillogenesis [86] as well as activate fibroblasts through FAK-integrin signaling in order to increase infarct stiffness and decrease likelihood of cardiac rupture [87]. Unlike periostin, the increase in collagen VI may be deleterious in cardiac remodeling. As a nonfibrillar collagen, collagen VI aids in organizing the fibrillar collagen I and III and anchoring them to the basement membrane [88]. Although seemingly important in maintaining structure, Luther et al. found that deletion of collagen VI in mice actually improves MI outcome as evidenced by reduced collagen deposition and decreased cardiomyocyte apoptosis in the infarct and remote regions [89]. Additionally loss of collagen XV in mice has been associated with increased tissue stiffness and irregularly organized cardiomyocytes [90] as well as a diminished inotropic cardiac response [91].

As expected, the different ECM components create a distinct environment which influences not only its mechanics and structural integrity but also its ability to bind cells and propagate signal. In one example of this, Atance et al. found that ECM composition can modulate deposition of collagen by fibroblasts [92]. It is important to understand these compositional changes and their functional impact when choosing materials for cardiac therapies.

3.3.3. Fiber structural changes

The organization of the newly deposited ECM is debated in literature based on the animal model used. For example, rats feature structurally and mechanically isotropic scars post-MI [93] while canines feature collagen fibers varying transmurally, −14° to 12° (endocardium to epicardium) [94]. Furthermore, porcine models have also been shown to have anisotropic scar formation post-MI with collagen fibers in the scar oriented at 30° relative to the circumferential axis [95]. However, such differences in the infarct fiber organization can be explained by regional mechanics in the infarcted environment [96,97]. Holmes et al. tested different infarct shape (circular, circumferential ellipsoid, longitudinal ellipsoid) and locations (apex or mid-ventricle) using a combined computational and experimental approach, finding that only infarct location significantly impacted scar orientation [97]. It has been shown *in vitro* that fibroblasts align with tension [98] and deposit collagen fiber along their axis [97]. In this way, the structural orientation of the scar can be explained by the local mechanics: infarct scars at the apex, in which the myocardium is stretched in both in the circumferential and longitudinal direction, are isotropic while infarct scars at the mid-wall, where the myocardium is stretched in the circumferential direction, are circumferentially aligned [97].

As previously mentioned, MI inhibits cardiac torsion. Marcelli et al. measured a significant decrease in the apical rotational angle in ovine models post-MI [99], likely caused by the change in myocardial fiber organization. Based on the structural fiber organization in healthy myocardium, dysfunction in the sub-epicardial region would cause reduced rotation with appropriate relaxation while dysfunction in the sub-endocardial would cause appropriate rotation with impaired relaxation [11,42].

3.4. Remodeling phase: chronic impacts

In the remodeling phase of MI, the mechanical properties of the scar decouples from the collagen content deposited in the region [56]. During this time, the scar itself continues to change as increased collagen crosslinking [100,101] and shrinkage within the infarct [100,102] occur.

The formation and dynamics of the infarct scar during the remodeling phase is especially significant when considering patient prognosis; the size, location and mechanical properties of the scar are critical in determining patient survival and quality of life [103]. In a study of fifty-two long-term MI survivors, the size of the scar had a positive correlation with left ventricle end diastolic and systolic volumes and negative correlation with ejection fraction [104]. Unsurprisingly, many studies support this observation reporting correlation of infarct size with decreased cardiac output, stroke volume and stroke work [105], increased risk of ventricular dilation [106] and worse prognosis [107]. Such statistics have inspired current clinical practices aimed at quickly restoring blood flow within the infarcted myocardium in order to limit infarct size, a goal which continues to be at the forefront in developing new therapies.

Mechanics within the scar also impact cardiac function. For example, at the early stages of MI the developing scar is extremely compliant, as cardiomyocytes slip past one another and collagen has not yet been deposited to reinforce the region. Unable to withstand the mechanical

load imposed on it, the infarct has an increased risk of rupture, with 10–20% acute MI suffering this fate [108]. On the other hand, increasing the infarct stiffness can be deleterious as it restricts the ability of the heart to contract efficiently and thus reduces cardiac output and blood flow [109]. Further, without active contractility, infarcts are prone to stretching and thinning which increase ventricular wall stress and can perpetuate into further remodeling, ventricular dysfunction, malignant arrhythmias and even HF.

In addition to the dynamics of the scar, an important consideration is its relationship with the surrounding surviving tissue, a region known as the border zone. High resolution reconstruction of the transmural collagen and cardiomyocyte organization within a rat ventricle shows lateral coupling between cardiomyocytes decreased by 65% over a 250 μm region within the border zone [110]. Additionally, Yankey et al. found unique regional strain profiles in the remote, adjacent and infarct zone, yet all consistently increased over the 8-week study. Increased wall stress has been shown to induce apoptotic pathways, with Yankey et al. reporting a positive correlation between regional strain and expression of the apoptotic proteins mitochondrial bax, cleaved caspase-3 and poly(adenosine diphosphate–ribose) polymerase [111]. By better understanding the mechanical dynamics in not only the scar but also the regions surrounding the healing infarct, therapies can be engineered to target surviving cardiomyocytes and preserve their function.

4. Treatments Based on Loading and Anisotropy

The idea of changing the mechanical environment of the myocardium to treat heart disease is not a new concept. For example, heart failure drugs such as angiotensin-converting enzyme (ACE) inhibitors and angiotensin II receptor blockers (ARBs) modulate the vasoconstriction of cardiovascular blood vessels by targeting angiotensin II, a potent agent for vasoconstriction [112]. Because resistance to flow is inversely related to the vessel radius (to the fourth power), drug-induced dilation of the blood vessel has a significant impact in lowering the afterload and increasing the stroke volume of the heart.

More recently, however, biomaterials are being used to modulate the mechanical environment of the heart post-MI. Such treatments predominately come in two forms: injection and epicardial restraints. From a mechanics standpoint, both injection and epicardial therapies work to thicken the infarcted area and reduce ventricular wall stress, based on the Law of Laplace. Injections have the advantage of being less invasive as compared to epicardial therapies, which may be more appealing in a clinical setting. However, injections utilizing cellular components suffer from low retention and engraftment within the infarcted area of the myocardium, with rates as low as 15% in rats injected with neonatal cardiomyocytes after 12 weeks [113]. Injected acellular biomaterials essentially act as a scar filler in order to improve ventricular wall thickness and cardiac function [114,115]. Such therapies feature a range of materials from natural polymers such as collagen [116], fibrin [117,118], decellularized porcine ECM [119–121], alginate [122,123], chitosan [5] to a variety of synthetic polymers [124,125].

Because the scope of this paper considers both the mechanical and structural understanding of the myocardium in developing post-MI therapies, the analysis will focus only on epicardial therapies, as their structure and anisotropy can be modulated in a way injection therapies have not been able to achieve. The subsequent section will entail a deeper analysis of the *in vitro* engineering techniques and *in vivo* implementation of these passive and active epicardial therapies in regard to their mechanical and anisotropic structural properties as well as their impact of cardiac function.

4.1. Passive epicardial therapies

Utilizing epicardial restraint as a therapeutic post-MI began with a procedure known as a cardioplasty, first performed at the Broussais Hospital, Paris in 1985. In the procedure, the latissimus dorsi muscle is wrapped around the epicardium and electrically stimulated [126]. Success of this procedure was found primarily in the passive restraint it provided to the heart. Although not in clinical practice today, this study stimulated further research into understanding the mechanisms underlying epicardial mechanical restraint and further development of such therapies, as outlined in Table 2.

Passive cardiac restraint therapies work by physically confining the ventricle in order to maintain its shape and size while providing mechanical reinforcement to the injured myocardium. This duality – confinement and reinforcement — reduce ventricular wall tension by physically preventing dilation or, in the case of MI, infarct expansion. *In vivo* and clinical studies demonstrate the ability of these passive devices to reduce ventricular diameter and improve cardiac ejection fraction [127,128]. Interestingly, cardiac restraint has also been shown to induce changes at the cellular level, which may in part explain how such devices not only prevent disease progression but improve hemodynamic cardiac function. Using canine HF models treated with an epicardial restraint device, Sabbah reports decreased cardiomyocyte hypertrophy, downregulation of the stretch proteins apoptosis-inducing factor and Bax, improved calcium handling and upregulation of α-MHC [129].

Two of the most extensively studied epicardial restraint devices are CorCap by Acorn and the HeartNet by Paracor. The Acorn CorCap, made by knitting polyester, features a unique geometry that provides bidirectional compliance, with greater support in the circumferential direction compared to the longitudinal direction **(Fig. 1A)** [130]. Preclinical studies in ovine models revealed improvement in global ventricular structure [127] and function [131] when treating tachycardia-induced HF as well as preserved cardiomyocyte length adjacent to infarcted myocardium when treating MI [132]. The CorCap proceeded to human clinical trials; however, due to insignificant cardiac functional improvements and extensive fibrosis on the epicardium which limited subsequent cardiac surgeries, the Food and Drug Administration (FDA) failed to advance the device [133,134]. The Paracor HeartNet is made out of nitinol wire mesh and can be administered using a fluoroscopic guide system in order to achieve a less invasive surgery as compared to the CorCap [135]. *In vivo* testing of the Paracor device with ovine models demonstrated reduced left ventricular dilation post-MI yet no functional improvement was observed [128]. The clinical trial featuring this device, Prospective Evaluation of Elastic Restrain to Lessen the Effects of Heart Failure (PEERLESS-HF), was suspended after six months when no significant improvement in cardiac function was observed over the control group [136].

Since the development of the CorCap and Paracor, many different natural and synthetic acellular materials have been utilized in epicardial patches for treatment post-MI [137]. For example, Ruiz-Lozano et al. engineered acellular scaffolds made of type 1 collagen, utilizing a plastic compression technique to achieve mechanical material properties similar to those of the native myocardium [138]. After *in vivo* evaluation of the patch using a murine MI model, Ruiz-Lozano et al. reported improved cardiac function; interestingly, histological and immunostaining analyses revealed infiltration of fibroblasts, smooth muscle cells, and epicardial cells into the acellular collagen patch. Additionally, porous acellular collagen sponges have been shown to promote angiogenesis upon implantation on rat hearts in cryoinjured regions [139]. Highly elastic materials have also been investigated to create acellular epicardial therapies due to their ability to withstand the dynamic mechanical nature of the heart. Wagner et al. report the use of acellular polyester urethane urea (PEUU), a highly elastic yet biodegradable material, which increased both transmural wall thickness and fractional area change in rat MI models [140] and increased transmural thickness, decreased end diastolic area and increased fractional area change in swine MI models [141].

The role of biodegradability in acellular epicardial patches has been investigated and shown to be advantageous in improving cardiac function. A study by Kitahara et al. featured polyglycolic acid as the

Table 2
Passive epicardial therapies.

Name/Material	Material Prop.	Model	Results	Ref.
Acorn CorCap Knit-Polyester	E_C = 10.55 MPa E_L = 9.70 MPa	*In vivo*- ovine Tachycardia-induced HF LAD permanent ligation	Increased fractional shortening, increased ejection fraction	[127, 131] [132]
		In vivo- canine Intracoronary embolization with polystyrene microsphere	Decreased CM length and volume in remote region	[152]
		Clinical trial, Phase II	Decreased LV-EDV; Increased LV systolic fractional area of shortening; Observed extensive fibrosis on the epicardium which limited subsequent cardiac surgeries and failed to advance due to insignificant cardiac functional improvements Provided inspiration for restraint therapies improvements and data supporting structural changes to the heart post-MI can improve its function	[133, 134]
Paracor HeartNet Nitinol wire mesh	N/a	*In vivo* – ovine LAD permanent ligation Rapid ventricular pacing Analysis after 6 weeks *Clinical trials*	Reduced LV dilation; no significant improvement in cardiac function failed to advance Provided example of epicardial restraint which can be administered using a fluoroscopic guide system to achieve less invasive surgery	[128, 136]
Compressed type 1 collagen patch	Elastic moduli ranging from 3000 to 10,000 Pa	*In vivo* -mice 10–13 weeks old C57BL/6J LAD permanent ligation	Decreased fibrosis, formation of interconnected blood vessels, patch infiltration by fibroblasts, smooth muscle cells, epicardial cells and immature cardiomyocytes (in comparison to infarcted hearts with no treatment)	[138]
PEUU	Pore size ranging 30–100 μm; Porosity 86%; Peak tensile stress/strain: 307 KPa/103% Initial modules: 704 kPa	*In vivo* – rat LAD permanent ligation *In vivo* – porcine Ischemia- reperfusion	Increased both transmural wall thickness and fractional area change Increased transmural thickness, decreased end diastolic area and increased fractional area change	[140, 141]
Biodegradable Polyglycolic acid	Peak tensile strength: 19.4 N (polyglycolic acid), 11.3 N (polyethylene terephthalate)	*In vivo* – canine LAD permanent ligation	biodegradable polyglycolic acid support showed increased ejection fraction, improved end diastolic pressure-volume relationship and decreased end diastolic wall stress as compared to the non-biodegradable treated group	[142]
Hydrogels				
Chitosan hydrogel	Storage modulus 5000-35,000 Pa based on %wt chitosan	*In vivo* – Wistar rats LAD permanent ligation	Cell infiltration and incorporation onto the epicardial surface Decreased fibrosis, decreased expression genes involved in fibrosis and stretch	[143, 144]
starch hydrogel with Ca $(NO_3)_2 4H_2O$ crosslinker	At gel point; viscoelastic	*In vivo* –rats LAD permanent ligation	High biocompatibility, slow degradation; decreased left ventricular dilation, increased ejection fraction and fractional shortening	[145]
poly-ethylene-glycol (PEG) and sebacic-acid-diacrylate (SDA)	Tested hydrogel and hydrogel coated on polyanhydroglucuronic-acid	*In vivo* –rats LAD permanent ligation	the scaffold with coated hydrogel resulted in increased ejection fraction and decreased left ventricular end-diastolic diameter	[146]
Anisotropic Acellular Therapies				
Modified Dacron	E_C = unrestricted E_L = 800–900 MPa	*In vivo*- Mongrel canines Temporary IVC occlusion LAD permanent ligation Immediate treatment Analysis 30 min post MI	Reduced EDV Improved systolic function without impairing diastolic filling	[151]
		In vivo – 77 Sprague Dawley rats LAD permanent ligation Immediate treatment Analysis 1,2,3,6 weeks post MI	Collagen alignment parallel to region strain	[96]
Electrospun PECUU fibers	D = 1.32 μm	*In vivo* – female Lewis rats MI permanent ligation 10 weeks post MI	N.S compared to MI in end systolic/diastolic area;	[6]

E_L = Young's Modulus in longitudinal direction.
E_C = Young's Modulus in circumferential direction.
EDV = End diastolic volume.
ESV = end systolic volume.

biodegradable material. The degradation of polyglycolic acid involves the conversion of glycolic acid to carbon dioxide and water, components which can be removed from the body via the respiratory system. Kitahara et al. reported the strength of the polyglycolic acid halved at 2 weeks *in vivo* and was lost at 4 weeks [142]. Kitahara et al. compared this biodegradable support to the non-biodegradable material, polyethylene terephthalate, in a canine model for MI. At 12 weeks, canines treated with the biodegradable polyglycolic acid support showed increased ejection fraction, improved end diastolic pressure-volume relationship and decreased end diastolic wall stress as compared to the non-biodegradable treated group. Such a biodegradable material overcomes the extensive scarring observed in devices such as the Acorn CorCap and Paracor HeartNet.

An important realization that arose from studying acellular epicardial restraint devices is the delicate balance between sufficient reinforcement and inhibition of cardiac function. If the passive restraint is too compliant, the energy generated by surviving, contracting cardiomyocytes will be wasted in stretching the material. This in turn will inhibit systolic function [56]. On the other hand, if the mechanical reinforcement is too stiff, the dynamic stretching and contraction of the myocardium during the cardiac cycle will be inhibited; functionally, this impacts the ability of the myocardium to utilize the Frank-Starling

mechanism to adjust cardiac output in response to increased blood volume. To address this delicate balance, hydrogel-based and anisotropic reinforcement has been studied as described below.

Acellular Hydrogels: Hydrogels have been explored as promising biomaterials for cardiac therapies due to their ability to mimic the native ECM, promote cells infiltration and maintain their shape. A variety of different hydrogel materials have been utilized in engineering epicardial therapies for MI treatment. Fiamingo et al. prepared acellular chitosan-based hydrogels as an epicardial therapy due to the material's biodegradability and ability to promote wound healing (Fig. 1B). When assessed *in vivo*, the chitosan hydrogel had low cell invasion when neutralized with NaOH; however, Domegngé et al. improved such invasion by increasing the degree of acetylation within the chitosan hydrogel [143,144]. Further, Lin et al. developed a viscoelastic epicardial patch made from ionically crosslinking a starch hydrogel with Ca $(NO_3)_2 4H_2O$. Finite element modeling and further testing *in vivo* illustrated the viscoelastic functionality of the patch was able to accommodate the cyclic mechanics of the heart and improve cardiac function at 4-weeks post-MI [145].

Vilaeti et al. developed a biocompatible and biodegradable hydrogel made out of poly-ethylene-glycol (PEG) and sebacic-acid-diacrylate (SDA). Interestingly, Vilatei et al. compared the hydrogel to a gauze-like material, polyanhydroglucuronic-acid, coated with the same hydrogel. *In vivo* testing showed attenuated remodeling in both systems; however, the scaffold with coated hydrogel resulted in increased ejection fraction and decreased left ventricular end-diastolic diameter suggesting the need to supplement the mechanical properties of hydrogels [146]. One of the major advantages of hydrogels is the ability to load hydrogels with biologics, such as growth factors, that further enhance the function of the heart post-MI. Although beyond the scope of this review, this topic is briefly discussed in Section 5.4 as to inspire continued research in this area and readers are referred to an excellent review by Li and Mooney [147].

Anisotropic Reinforcement: Development of innovative technologies in material engineering has afforded the ability to precisely control the structure and mechanics of material-based therapies, both of natural and synthetic origin. Physical cues can have a significant impact on cardiac function and remodeling post-MI, motivating studies to investigate anisotropic reinforcement to the heart through acellular epicardial patches and in engineering cardiac tissue (as will be discussed in the next section).

Several prominent groups have contributed to the understanding, engineering and implementation of anisotropic cardiac therapies. Using a finite element model, Estrada et al. and Fomovsky et al. from the Holmes Group as well as Voorhees and Han observed increased cardiac function through longitudinal reinforcement of the ventricular wall post-MI [148–150]. These models illustrate that isotropic stiffening of the infarct improves systolic function, most likely by minimizing energy dissipation in the infarct region, but negatively impacts diastolic filling. The original hypotheses surrounding longitudinal restraint post-MI was intuitive: mechanical restraint in the longitudinal direction would provide appropriate reinforcement while mechanical freedom in the circumferential direction would allow for increased myocardial stretch, diastolic filling and contractile ability through the Frank-Starling mechanism. However, the opposite was found *in vivo*: longitudinal enforcement improved systolic, as opposed to diastolic, function. In these studies, Fomovsky et al. used a modified Dacron path which contained longitudinal slits so motion in the longitudinal direction was supported but motion in the circumferentially direction was unrestricted. *In vivo* testing using canines post-MI illustrated improved systolic function without hindrance of diastolic function [151]. Further computational modeling by this group found that such longitudinal reinforcement improved systolic function post-MI by reducing the magnitude of fiber stretch during diastole and stress during systole while also redistributing these peaks from the endocardial surface toward the mid-wall, where the myocardial fibers are circumferentially distributed and the generated torque is greater [149].

In conjunction with anisotropy, appropriate material properties may play a key role in achieving the benefits associated with longitudinal reinforcement *in vivo* (**Fig. 1C**). D'Amore et al. found no functional cardiac improvement with circumferential or longitudinal epicardial reinforcement post-MI in rat models compared to controls when using electrospun polyester carbonate urethane urea (PECUU) fibers [6]. Upon explant 10 weeks post-MI, the circumferential and longitudinal patches displayed similar bi-axial mechanical properties, suggesting changing PECUU fiber mechanics or geometry within the dynamic native cardiac environment.

4.2. Active epicardial therapies

It is estimated that 1 billion cardiomyocytes are killed during myocardial infarctions with hemodynamically significant outcomes [153]. An important consideration when engineering therapies to compensate for such a devastating loss is the regenerative capabilities of the heart itself. Using radiocarbon (^{14}C) birth dating, researchers have been able to estimate the cardiomyocyte turnover in humans to be between 0.5 and 2% [154–156]. However, this rate is dependent on age, with the lowest regeneration (<0.5%) occurring in elder populations (>75 years) [154].

The point of discussing cardiomyocyte regeneration is to highlight the fact that cardiomyocytes lost during MI are not able to be replaced at a rate relevant to improving cardiac function [154–156]. Once they are lost, the infarcted area essentially loses its ability to contract. Although there are benefits in utilizing acellular epicardial therapies – full characterization of the material, stable shelf life and defined scaling up procedures – they fail to directly address the loss of functional, actively contracting myocardium. Addressing this loss is especially important for large infarcts, in which the death of cardiomyocytes and sudden loss of force generation are too significant for passive therapies to have functional benefits.

This need for an active component in MI treatments was highlighted in an unexpected way through the clinical studies of the cardioplasty procedure. During the procedure, pacemakers were implanted in order to stimulate the latissimus dorsi on the epicardial surface. After 10 years, the pacemakers began to die resulting in cessation of latissimus dorsi stimulation. Interestingly, patients with failed pacemakers presented with symptoms of HF; however, when the pacemaker batteries were replaced and stimulation was recovered, patients made a gradual recovery [126]. Thus, the ability to incorporate active components within epicardial restraint devices is a promising field filled with exciting research and advancements.

4.2.1. Active robotic epicardial therapies post-MI

Advancements in robotics have ushered in the ability to artificially engineer the active component of the heart, as illustrated in Table 3. One such therapy in current use as a bridge-to-transplantation is the left ventricular assist device (LVAD) (**Fig. 1D**). The LVAD is a mechanical pump that helps a failing left ventricle pump blood to the aorta. In the REMATCH (Randomized Evaluation of Mechanical Assistance in the Treatment of Congestive Heart Failure) trial, patients treated with an LVAD essentially doubled their survival (from 25% to 52%) after one year [157]. Another mechanical device, SynCardia Total Artificial Heart (TAH), is currently the only FDA-approved total artificial heart (**Fig. 1E**). Unlike the LVAD, which is implanted adjacent to left ventricle, the TAH requires resection of both ventricles and replaces them with artificial ventricles composed of biocompatible plastic. More than 1700 TAHs have been implanted in patients around the world with a success rate of 67.6% at 12 months (53.5% patients receiving a transplantation and 14.1% alive on the TAH device) [158].

Despite these benefits, the LVAD and TAH require lifestyle adjustments and can have severe complications. First, these devices require external, battery-operated machinery, weighing approximately five

Table 3
Active robotic epicardial therapies post-MI.

Type	Material Prop.	Model	Results	Ref.
LVAD	Pump implanted adjacent to failing LV to circumvent blood flow to the aorta	*Clinically used as a bridge-to-transplantation therapy*	Increased survival from 25% to 52% at one year with LVAD	[157]
TAH	SynCardia; Polyurethane	*Clinically used as a bridge-to-transplantation therapy*	67.6% patients at 12 months either underwent heart transplant or alive on the device	[161] [158]
DCC	Helical and circumferential McKibben soft actuators	*In vivo* - porcine Esmolol induced HF (reduced cardiac output to 45% of baseline)	Increased Aortic Flow rate Recovered cardiac output to 97% of baseline	[7]
DCC	Individual McKibben-based actuators with elastic sleeve	*In vivo* – porcine Esmolol induced HF	Mechanical coupling between implant and native heart	[162]
DCC	Elastomeric polyurethane (PU) open-celled foam with inside coated with PU elastomer and outside coated with PU elastomer + 5% chopped carbon fiber	*Ex vivo* – porcine	0.12 L/min peak flow at a frequency of 60 beats/min	[164]
VAD	2 McKibben soft actuators, Brace Bar and Anchoring system	*In vivo* - porcine Permanent LAD (aortic flow reduced to 39%) Coronary occlusion through polystyrene microbeads (aortic flow reduced to 56%)	Increased aortic flow; Decreased end diastolic LV pressure; Increased peak LV pressure	[163]

LVAD = left ventricle assist device.
TAH = total artificial heart.
DCC = direct cardiac compression.
VAD = ventricular assist devices.

pounds, which must constantly be carried by the patient and charged by a consistent power source. Additionally, because the devices interact directly with blood, patients must be treated with blood thinning drugs in order to decrease the risk of thrombosis within the device [159]. Anticoagulants pose an increased risk of bleeding, and when analyzing 200 patients with LVADs implanted between 2006 and 2014, gastrointestinal bleeding was the most common complication (21% of patients analyzed) [160]. Further complications are prominent in patients on TAH for long-term use (>12 months) with 10% patients experiencing device-related technical problems, 53% experiencing systematic infection and 14% experiencing a hemorrhagic event [161].

One design solution overcoming the issue of clotting as seen in long-term use of LVADSs and TAHs is the use of soft actuators implanted on the epicardial surface of the heart **(Fig. 1F)**. Because the actuators are not in direct contact with blood, the use of anticoagulants becomes unnecessary. Additionally, by utilizing soft-bodied robotic devices the mechanical and structural properties of not only the material but force generation can easily be tuned. By positioning actuators circumferentially and helically on the epicardial surface, compression and twisting, respectively, can be achieved to mimic the torsion of a healthy heart [7,162,163]. Further developments are being made such as synchronization of the robotic cardiac sleeve with the native heart through pressure readings from catheters placed in the left ventricle [162] as well as 3D printing of actuating epicardial implants from patient MRI or CT scans [164]. Payne et al. even added an elastic sleeve over the epicardial actuators, which upon depressurization, use its stored elastic energy to ensure proper recoiling of the device [162].

4.2.2. Active cellular epicardial therapies post-MI

The ultimate goal of treating MI is to replace the healthy myocardium that was destroyed and restore cardiac function. An ideal approach to this treatment is replacing the infarcted scar tissue with healthy, contracting cardiomyocytes. Cardiomyocytes engineered into tissues which can then be implanted on the epicardial surface of the infarcted area can replace the contractile myocardium lost during MI while reducing or eliminating risks such as thrombosis, external sources of power and machine failures observed in robotic-based epicardial devices.

The functional benefits of using cells, particularly in epicardial patches, for MI treatments has been well established through *in vivo* testing [165,166]. However, one of the biggest limitations in using cardiomyocytes, specifically those derived from human pluripotent stem cells (hPSCs), is their immature function compared to adult cardiomyocytes [167–170]. A recent study using single-cell RNA sequencing across different datasets reports that PSC-derived cardiomyocytes mature only up to a fetal stage [171]. Methods being used to promote maturation of these cardiomyocytes include physical, biochemical, electrical and mechanical conditioning. By engineering scaffolds and/or environments with the appropriate mechanical and anisotropic components, the physical cues promote cardiomyocyte alignment, which as discussed, improve their contractile function. Although there are many techniques for developing these environments, this review will focus only on those that modulate the mechanical and anisotropic properties to create 3D tissues, as they are imperative in translation to an epicardial therapy. The techniques to engineer these composite systems will be discussed briefly and supplemented with Table 4, which outlines their functional impact in greater detail.

4.2.2.1. Scaffolds. Scaffolds are an important resource in engineering cardiac tissue. With the ability to precisely measure and control scaffold mechanics and structure, their use in cardiac tissue engineering serves as a vital tool in better understanding cardiomyocyte-material interactions and engineering physiologically relevant, cardiomyocyte-based epicardial therapies.

Decellularized Constructs: Intuitively, an optimal structural and mechanical environment for cardiomyocyte culture is the myocardium itself. A variety of different tissue types and techniques have been utilized in decellularization of tissues for cardiac tissue engineering applications **(**Fig. 1G**)**. For example, full heart decellularization and recellularization has been investigated to create tissue-engineered organs [8,172,173]. In this review, decellularization scaffolds to create engineered cardiac tissue patches will be discussed; however, additional methods and applications are extensively reviewed by Bejleri and Davis [174].

Techniques have been developed to decellularize the myocardium without disrupting its native structure and composition [121]. Schwan et al. utilized a commercial CO_2 laser to cut sheets of decellularized porcine myocardium and create precisely defined scaffolds upon which cardiomyocytes could be cultured [175]. Alternatively, Balzeki et al. used a vibrotome in order to section 300 μm thick rat or porcine myocardium which could be decellularized and seeded with cardiomyocytes [176].

In addition to decellularized myocardial ECM, decellularized pericardial tissue has been identified as a potential scaffold for cardiac tissue engineering [177,178]. The pericardium is a membrane which encloses the heart and serves to protect and anchor it. Decellularized bovine pericardium has been widely used in cardiac surgery and for replacement heart valves when processed and crosslinked to increase durability and reduce immunogenicity. This material is advantageous as it has a

Table 4
Active cellular epicardial therapies post-MI.

Fabrication	Scaffold Properties	Engineered Cardiac Tissue	Model	Results	Ref.
Laser cutting decellularized myocardium	Myocardium was cut in 150 μm slices; native fiber angle was oriented either parallel or 90° relative to the long axis of the tissue	Neonatal rat cardiomyocytes Human embryonic stem cells (hESCs) Induced pluripotent stem cell (hiPSC) 100 µL cell in media 10 million cells/ml	In vitro	Compared to transverse tissues, longitudinal orientation produced peak stress 420% greater. Maximum peak stress of 6.5 mN/mmˆ2 Average peak stress of 2.2 mN/mmˆ2 Time from peak stress to 50% relaxation: 168 ms Time to peak stress: 181 ms (at a 1 Hz pacing frequency)	[175]
Directional freezing of cECM (cardiac ECM) and silk	Dynamic modulus in the range of 25–50 kPa in the longitudinal direction	ESC-derived cardiomyocytes: 5×10^5 cells/mL in media HL-1 continuously proliferating cardiomyocytes from atrial tumor: 1×10^6 cells/mL in media 100 µL/construct Scaffold volume is 125 mm^3	In vitro 1 week	Acellular subcutaneous implant; 99% cell infiltration Compared to isotropic scaffold (using HL-1 cells): Increased connexin 43, increased MHC content Compared to aligned without cECM (using hESC): Increased integrin β1, islet-1, and cardiac troponin I	[182]
Microgrooves from PDMS seeded with collagen-chitosan-CM	10,20,100 µm microgrooves Height ~ 220 um	neonatal ventricle myocytes (Sprague-Dawley rats) Collagen I: 0.19 mg/mL and Chitosan = 9.5 mg/mL	In vitro Day 6	Increased alignment, lower excitation threshold, increased success of beating (100%) for 10 µm microgrooves For 10,20,100 µm unstimulated tissues, respectively: Excitation threshold ~1 V/cm, 2.5 V/cm,2 V/cm Maximum capture rate ~ 4Hz, 5Hz,4.5 Hz	[185]
Heat wrinkling of palladium metal and polystyrene polymer	PDMS with laminin and fibronectin coating wrinkle thickness: 800 nm −1 µm depth: nm to ~3 µm	murine neonatal cardiomyocytes human embryonic stem cell induced cardiomyocytes	In vitro Days 1,2,3,7	Increased alignment (alpha actin, cardiac troponin I)	[187]
Ellipsoid pores introduced through post size	Controls, 0.6 mm ellipsoid pores and 1.2 mm ellipsoid pores	neonatal ventricle myocytes (Sprague-Dawley rats) hydrogel solution containing 2 mg/mL fibrinogen, 10% Matrigel, 5×10^6 cells/ml, and 1 U/ml thrombin	In vitro 2 weeks	Increased alignment with larger pores No significant different in transverse conduction velocity Control CV = 17 cm s−1 AR = 1.33 Pore = 0.6 mm CV = 20 cm s−1 AR = 1.3 Pore = 1.2 mm CV = 26 cm s−1 AR = 1.6	[184]
Laser-etched acrylic to fabricate PDMS molds	Single post and multiple posts at lateral ends of the engineered tissue; Rectangle, triangle and diamond and striped shaped features with different aspect ratios to modulate cell alignment	Induced pluripotent stem cell (hiPSC) Minimum: 10 × 3 mm Maximum: 2 × 1.5 cm	In vitro In vivo	Achieved conduction 0.17 mm/ms along border and 0.04 mm/ms in the transverse direction Action potential of 290 ms Diamonds, triangles and stripped designs provided enhanced cardiomyocyte alignment; but breakage of stripped and difficulty in loading triangular without introducing bubbles	[186]
Electro-hydrodynamically printed micro-lattices with PCL	Spacing: 200,400,600,800 μm Heights: 154 µm, 307 µm and 568 µm	neonatal ventricle myocytes (Sprague-Dawley rats) Collagen 1 = 3 mg/ml Cell density = 1.6×10^6 cells/ml	In vitro Hours	Proof-of-concept; successfully demonstrated the possibility to align multilayer cellular scaffolds	[189]
poly(glycerol sebacate) (PGS) honeycombs	Overlapping two 200 µm by 200 µm squares at 45° followed by excimer laser ablation Accordion honeycombs: Rectangular honeycombs:	neonatal ventricle myocytes (Sprague-Dawley rats) 36×10^6 cells/cm^2. Construct: 5 × 5 mm	In vitro 1-week	Accordion honeycombs: ET_L = 0.9 V ET_T = 0.7 V Rectangular honeycombs: ET_L = 1 V ET_T = 0.85 V	[188]

(continued on next page)

Table 4 (*continued*)

Fabrication	Scaffold Properties		Engineered Cardiac Tissue	Model	Results		Ref.
	200 × 200 μm E_L = 195 kPa E_T = 57 kPa	400 × 200 μm E_L = 206 kPa E_T = 117 kPa					
Electrospinning w/stretch PCL fibers	Random D = 14 μm MTS = 2.9 MPa E = 0.72 MPa EB = 426%	Parallel D = 7 μm MTS = 10.2 MPa E = 1.81 MPa EB = 426%	hiPSC-derived cardiomyocytes 1 × 10^6 cells/scaffold in media Scaffold: 6 mm diameter, 0.1 mm thick	In vitro 12 days post seeding	Upregulation of MYH7 expression, maximum spontaneous velocity and calcium handling phenotype CASQ2 Random CV = 2.4 μm/s 55 BPM paced 1 Hz SL = 1.3 μm	Parallel CV = 3.8 μm/s 60 BPM paced at 1 Hz SL = 1.6 μm	[200]
Electrospinning PLGA w/ stretch	D = 0.9–1 um Porosity = 71–78%		neonatal ventricle myocytes (Sprague-Dawley rats) 400,000 cells/cm^2. 12 × 7 × 0.2 mm	In vitro	Increased cardiomyocyte elongation evidenced by SEM and confocal imaging		[199]
Electrospinning polymethylglutarimide (PMGI)	Ave diameter: 400 nm - 1.2 μm Fiber distance: 200, 100, 50, 20–30 μm		neonatal ventricle myocytes (Wistar rats) 2 × 10^5 cells/cm^2. Scaffold dimensions: 2–20 mm in width and 20–25 mm in height	In vitro	Greatest alignment when fiber spacing <30 μm longitudinal-to-transverse velocity ratio of 2.0		[198]
Electrospinning PVDF	Aligned: D = 0.59 of E = 27.9 MPa YS = 6.5 MPa	Random: D = 1.2 um E = 15.9 MPa YS = 3.5 MPa	neonatal ventricle myocytes (Sprague-Dawley rats) 5 × 10^5 cells in media 15 μL/construct	In vitro Day 7,14	Increased alignment (alpha actinin staining) Increased cellular elongation Increase sarcomere length		[195]
Electrospinning Albumin	Aligned: E = 1.22 MPa D = 1.48 μm (10% albumin); 6.2 μm (14% albumin)	Random: E = 0.43 MPa D = 1.53 μm (10% albumin); 5.13 μm (14% albumin) Pa	neonatal ventricle myocytes (Sprague-Dawley rats) 5 × 10^5 cells/10 μL media suspension	In vitro Day 3, 7	Higher beating rate Higher contraction amplitude		[196]
Electrospinning PCL/Gelatin	E_L = 500 kPa E_T = 74 kPa		hiPSC-derived cardiomyocytes 90,000 cells/mm^3 Half ellipsoidal (a = b = 4.5, c = 9 mm, V = 500 μL, thickness = 0.1 mm)	In vitro 14 days post seeding analysis	EF = 2% SW = 0.05 mmHg/μL Structural arrythmias model proof-of-concept		[197]
Wet spinning collagen fibers	hydrated collagen micro-fibers: E = 0.73 MPa UTS = 0.05 MPa 30° fiber angle: E_L = 22.28 kPa E_T = 4.92 kPa	60° fiber angle: E_L = 11.40 kPa E_T = 6.85 kPa	hiPSC-CM 15 × 10^6 cells/mL 1.2 mg/mL collagen I. 50 μL/construct	In vitro	Constructs compacted to 38.4% by 96 h Ability to create precisely define collage microfiber scaffolds		[2]
Wet spinning fibrin threads	140 μm spacing between fibrin micro-threads Elastic modulus: 5% fiber volume = 20.6 kPa 11% fiber volume = 46.4 kPa 22% fiber volume = 97.5 kPa		neonatal ventricle myocytes (Sprague-Dawley rats) hydrogel solution containing 4 x 10^6 xcells/mL, 1.6 U/mL thrombin, and 3.1 mg/mL fibrinogen	2 and 3-day old neonatal Sprague–Dawley rats	Improved alignment compared to no fibers. CMs could sense stiffness and direction of fiber up to 100 μm.		[202]
Wet spinning fibrin threads	Aligned: UTS = 800 kPa	Random: UTS = 400 kPa	neonatal ventricle myocytes (Sprague-Dawley rats) 5 × 10^6 cells/mL Fibrin hydrogel (of 3.3 mg/mL)	In vitro 2 weeks	Aligned: Contractile force = 1.3 mN	Random: Contractile force = 0.47 mN	[201]
laser-based stereolithography printing	gelatin methacrylate (GelMA) and polyethylene glycol diacrylate (PEGDA) different fiber width (100, 200 and 400 μm), fill density (20,40,60%), fiber angles (30°,45°,60°) and different stacking layers (2,4,8 layers).		hiPSC-CM Printing mixture contains: 1 × 10^6 per ml of hiPSC-CMs with 5% GelMA and 15% PEGDA	In vitro In vivo	improved adhesion to the epicardial, angiogenesis and cell infiltration in the cellularized constructs		[203]

E_L = Young's Modulus in longitudinal direction.
E_T = Young's Modulus in transverse direction.
D = Diameter.
MTS = Maximum Tensile Strength.
UTS = Ultimate Tensile Strength.
EB = % Elongation of break.

YS = Yield Strength.
CV = Conduction velocity.
SL = sarcomere length.
EF = ejection fraction.
SW = stroke work.
AR = Anisotropic ratio.
BPM = beat per minute.

fibrous structure rich in elastin and collagen, affording it the ability to withstand mechanical stress while also having the structurally integrity to be sutured onto the heart [179]. Perea-Gil et al. compared the function of decellularized myocardial tissue and pericardium as a scaffold for cardiac tissue engineering through *in vitro* and *in vivo* testing [178]. Perea et al. performed proteome characterization of the myocardial and pericardial decellularized ECM, reporting enrichment of matrisome proteins and ECM components as well as better cell penetration and retention in the re-cellularized pericardium as compared to the re-cellularized myocardium. Further *in vivo* studies showed both re-cellularized scaffolds, regardless of origin, were able to integrate into the host and improve ventricular function in treating swine post-MI hearts. The creativity in utilizing different decellularized materials as cardiac scaffolds may best be exemplified by Gaudette et al., who utilize decellularized plants as a cardiac tissue scaffold. This "green" technology features decellularized spinach leaves, which are able to retain cardiomyocytes even without ECM coating [180,181].

Other approaches utilize decellularized myocardium in conjunction with additional materials to create hybrid scaffolds while maintaining anisotropy. For example, Stoppel et al. combined silk with solubilized decellularized myocardial ECM and, through a directional freezing approach, achieved a structurally anisotropic scaffold [182]. Additionally, Smoak et al. used decellularized skeletal muscle ECM with hexafluoro-2-propanol (HFIP) in order to electrospun the solution into randomly oriented fibers [183]. Although decellularized myocardial ECM captures the environment, structure and composition of the native heart, and hydrogels formed from it maintain the compositional complexity, it is very challenging to recellularize at a high cell density and may not be sustainable.

Topographical Cues: Technologies utilizing topographical design features have been developed to engineer scaffolds that recapitulate physiologically relevant mechanical and structural cues in order to promote cardiomyocyte function. Structural ridges and grooves create lanes which physically constrain cardiomyocyte spreading and promote alignment [184–189]. Topography is often introduced to a system through replica molding in which negative masters are created and used to fabricate elastomeric molds, typically formed from poly(dimethylsiloxane) (PDMS), on which cardiomyocytes or engineered cardiac tissues are cultured. Thus, the technique and design involved in fabricating the negative molds directly impacts the environment of the cardiomyocytes (Fig. 1H). Photolithography has frequently been used in creating the structural designs of these negative molds [9,184,185]. However, recent advancements have been made in order to overcome the time-consuming, expensive and technical process of photolithography. For example, Munarin et al. utilized laser-etched acrylics as negative masters, illustrating the ability to create PDMS molds of different size, shape and topographical design, while achieving a resolution of ~200 μm [186]. Additionally, Luna et al. developed a technique which exploits the stiffness differences between a polymer sheet and metal; upon heating of this system, the gold-palladium metal film buckles while the polystyrene polymer retracts to cause the formation of wrinkles [187]. The scale of the wrinkling can thus be modulated by the thickness of the metal film and further used as a negative master to create PDMS molds. One limitation of using specifically PDMS, especially if considering the reuse of scaffolds, is their ability to absorb small, hydrophobic molecules and proteins [190]. To overcome this, printing of polycaprolactone (PCL) to create precisely defined micro-lattices [189] as well as overlapping scaffold layers and using excimer laser microablation to create an accordion-like honeycomb design [188] have been developed.

Fibrous Scaffolds: Frequently when engineering tissues, hydrogels are utilized due to their ability to mimic the native ECM, entrap high concentration of cells and maintain their shape. However, these hydrogels, especially those of natural origins are mechanically weak and their structures cannot be intrinsically defined [191,192]. This is illustrated in the work of Munarin et al. and Bian et al. in which the topographical features to promote anisotropy introduces holes within the engineered cardiac tissue, resulting in increased tissue fragility and compromised mechanical integrity [184,186]. In order to modulate both the mechanics and anisotropy while maintaining mechanical integrity, researchers encapsulate fibers within cell-hydrogel mixture. The mechanical properties of such fibers can be modulated based on the chosen material and density of fibers while its structural anisotropy is largely based on technique used to fabricate them. In electrospinning, for example, fiber alignment can be induced by changing device parameters such as using a rotating mandrel collection device and modulating rotational speed [193–197] the use of electrodes in front of the collection device [198] or post-processing conditions, such as uniaxial stretching [199,200].

Despite the advantages of electrospinning, one major drawback is the harsh conditions which limit the material which can be utilized. An attractive alternative is wet spinning, in which a polymer dissolved in a solvent solidifies into a fiber upon precipitation out of its solvent. Recently, our lab has developed a system in which wet-spun collagen fibers are collected on a rotating mandrel in a way that allows fiber spacing, orientation and size to be modulated (Fig. 1I) [2]. Wet-spun fibrin fibers have also been created for use as cardiac tissue scaffolds through coextrusion of fibrinogen and thrombin [201,202].

Fiber anisotropy can also be recapitulated through 3D printing technologies. Using a gelatin methacrylate (GelMA) and polyethylene glycol diacrylate (PEGDA), Cu et al. utilized laser-based stereolithography printing to create anisotropic scaffolds to which cardiomyocytes could be seeded [203]. GelMA was used due to its ability to be crosslinked with a photoinitiator as well as its ability to promote cell attachment while the PEGDA solution was mixed with GelMA to control its swelling volume and increase the mechanical integrity of the scaffold. Cui et al. printed a variety of designs featuring different fiber width (100, 200, 400 μm), fill density (20, 40, 60%), fiber angles (30°, 45°, 60°) and stacking layers (2, 4, 8 layers). When comparing cellular and acellular constructs in rat MI models, Cu et al. reports improved adhesion to the epicardium, angiogenesis and cell infiltration in the cellularized constructs [203].

4.2.2.2. Conditioning environment. In recapitulating the native cardiac environment, the role of the heart's dynamic mechanics has been investigated to promote maturation of engineered cardiac tissue.

Static and stepwise mechanical stretching of engineered cardiac tissue refer to an initial stretching of the tissue or a stepwise increase in the percent stretch over time. For example, static stretching of engineered can easily be introduced to tissue systems through posts at the tissue edges [184,186,204]. Many studies have illustrated the beneficial effect of cardiomyocytes static stretching such as stabilization of cardiomyocyte myofibrillar structure (5% static stretch) [205] and increased gene expression of c-fos and ANP (15% static stretch, 30 min) [206].

Dynamic stretching, on the other hand, refers to cyclic mechanical stretching which mimics the filling of the ventricles with blood. Fink

et al. utilized phasic unidirectional stretch of engineered cardiac tissue for 6 days in culture, reporting induction of cardiomyocyte hypertrophy and functional improvement. More specifically, Fink et al. observed improved cardiomyocyte organization, increased atrial natriuretic factor mRNA and alpha-actin, increased force of contraction (up to four-fold higher than un-stretched engineered cardiac tissue), increased cell length and width, longer myofilaments, increased mitochondrial density and accelerated contraction kinetics [207]. Salameh et al. further studied the localization of gap junctions in response to mechanical stimulation, finding that cyclic mechanical stretch of neonatal rat cardiomyocytes polarized connexin 43 and N-cadherin to the cardiomyocyte ends [208]. Additionally, Tulloch et al. reported a two-fold increase in cardiomyocyte proliferation as well as increased alignment, myofibrillogensis and sarcomeric banding in 3D engineered cardiac tissues undergoing uniaxial mechanical stress [209]. Zimmerman et al. illustrated the functionality of mechanically stretched engineered cardiac tissue by implanting the constructs *in vivo*, finding the tissues were able to survive and improve cardiac function in rats post-MI [210]. Mechanical stimulation can also take the form of compressive strain. For example, Shachar et al. applied compression (1 Hz, 15% strain) combined with fluid shear stress (10^{-2} to 10^{-1} dyn/cm^2). Compression was applied to engineered cardiac tissues for 4 days, 30 min each day with Shachar et al. reporting increased expression of connexin 43 and elevated secretion of basic fibroblast growth factor and transforming growth factor-β [211].

Sophisticated systems to induce phasic mechanical stimulation are available. For 2D cultures, the Flexecell Strain Unit (Flexcell Int., Hillsborough, NC, USA) is commonly used. In this system, a vacuum pressure is applied to the bottom of the culture plate to induce deformation and thus mechanical stretch of cells cultures above. Additional 3D systems have been developed, such as the Biostretch apparatus (ICCT Technologies, Markham, ON, Canada) in which different protocols can be programmed [212]. Additionally, Zimmermann and Schenider-banger developed a different approach to engineering their tissue with mechanical stretch, creating circular cardiac tissues placed over two mechanically-controlled poles that could provide unidirectional, cyclic stretch (10%, 2Hz) [213]. Atcha et al. also describe a low cost method to fabricate a uniaxial cell stretcher using a servomotor [214]. Further innovation has led to the creation of bioreactors which can be tuned and used to scale up technologies. Such bioreactor development for cardiac tissues is reviewed in great detail by Govani et al. [215].

Mechanical stretch of engineered cardiac tissue has also been used in conjunction with electrical stimulation at physiological frequencies. For example, Black et al. tested several different electromechanical protocols, reporting that beginning mechanical stretch before electrical stimulus resulted in tissues with the highest contractile force. This delay is hypothesized to be most effective as it mimics the native mechanical environment [216]. Further, Godier-Furnémont et al. achieved a positive force-frequency relationship in their engineered cardiac tissue when conditioning with mechanical and electrical stimulation at physiological frequencies [217]. Lluciá-Valldeperas et al. developed a device to provide mechanical and electrical stimulation which can be sterilized, used in a standard culture plate and tuned appropriately [218,219].

Further, electrical conditioning has also been used in conjugation with topographical cues to promote cardiomyocyte alignment. Several studies report that topographical cues were a stronger determinant of cardiomyocyte orientation over electrical stimulation, although electrical stimulation further improved cardiomyocyte elongation in the presence of topographical cues [185,220,221]. Au et al. further investigated the molecular mechanisms at play when utilizing both electrical stimulation and topographical cues, reporting that cardiomyocyte orientation and elongation was abolished by cytochalasin D, an inhibitor of actin polymerization, and partially inhibited by LY294002, an inhibitor of the phosphatidyl-inositol 3 kinase (PI3K) pathway. However, electrical stimulation reversed the impact of LY294002 and thus could partially recover signaling of the phosphatidyl-inositol 3 kinase (PI3K) pathway [221].

4.2.2.3. Additional considerations in engineering cardiac tissue. This review primarily focuses on engineering techniques and technologies to create material that recapitulate the heart's physiological structure and mechanics. However, there are additional considerations in engineering cardiac tissue that can significantly impact the mechanical function and anisotropic structure of cardiomyocytes. Although not the focus of this review, a few of such components will be briefly assessed to underscore their importance and inspire continued research into better understanding the culturing conditions for creating functional cardiac tissue.

Heterotypic Cell Interactions: The cardiac cellulome is incredibly diverse. Although responsible for 70–80% of the volumetric fraction of the heart, cardiomyocytes comprise only one-third of the cardiac tissue by cell number with endothelial cells and cardiac fibroblasts as the majority non-cardiomyocyte cell populations [222,223]. Utilizing single-cell RNA sequencing, Skelly et al. extensively characterized the transcriptional profile of murine non-myocytes to quantify such cellular diversity and gain insight into the intercellular relationships which allows for proper heart function. In the study, Skelly et al. identified 12 distinct cell cluster: endothelial cells (Cdh5,Pecam1); fibroblasts (Cola1, Pdgfra, Tcf21); granulocytes (Ccr1, Csf3r, S100a9); lymphocytes (Ms4a1,Cd3e,Klrb1c,Ncr1); pericytes (P2ry14, Pdgfrb); macrophages (Adgre1, Fcgr1); dendritic cell (DC)-like cells (Cd209a); schwann cells (Plp1,Cnp); and smooth muscle cells (Acta2, Tagln) [224]. Such an analysis provides an important resource for the cellular composition of the heart and serves to stimulate research into the role of non-cardiomyocyte cell population on cardiac tissue function.

Understanding the diverse cellular landscape of the heart aids in cardiac regeneration as heterotypic cellular interactions have been shown to impact the phenotype and function of engineered cardiac tissue. For example, co-culture of cardiomyocytes with endothelial cells [204,209,225–227], human marrow stromal cells [209,226] and pericyte cells [228], have been shown to support and enhance vascularization in engineered tissue *in vitro* and *in vivo*. More recently, however, the mechanical and structural impact of non-cardiomyocyte on engineered cardiac tissue function is being investigated. For the scope of this review specific examples will be discussed as it pertains to cardiac mechanics and structure; however, further research into multi-cellularity in engineering cardiac tissue is reviewed extensively by Owen and Harding [229].

One key cell type in in the cardiac cellulome is fibroblasts. Cardiac fibroblasts play a key role in providing structural maintenance and support by providing organization in the cardiac ECM.

In engineering cardiac tissues, fibroblasts have been shown to increase compaction of the tissue, contractile force and cardiomyocyte alignment [230–233]. Rupert et al. extensively investigated the effects of co-culturing hiPSC-derived cardiomyocytes with adult human cardiac fibroblasts (hCFs) in 3D engineered tissues, finding that the number and activation state of hCFs significantly modulates hiPSC-cardiomyocyte function [232]. Rupert et al. reports that engineered cardiac tissue supplemented with 5% hCFs displayed increased tissue compaction and up to three-fold increased contractility compared to tissues composed of only hiPSC-cardiomyocytes. However, increasing the percentage of hCFs to 15% increased ectopic activity and spontaneous excitation rate while supplementing the engineered cardiac tissue with hCFs that underwent myofibroblast activation ablated the functional benefit observed with 5% hCFs. Interestingly, these beneficial results are not reproduced with neonatal human dermal fibroblasts, suggesting the important and specialized role of cardiac specific fibroblasts. Additionally, Beauchamp et al. used CFs in conjunction with hiPSC-derived cardiomyocytes in engineering cardiac spheroids, reporting increased maturation and function [233]. Interestingly, Beauchamp et al. utilized SEM and TEM to characterize the surface and ultrastructure of the cardiac spheroids with CFs, reporting smoother spheroid surface with CFs as well as

well-formed intercalated disc-like structures and cell-cell contacts between non-myocytes and hiPSC-derived cardiomyocytes.

Recently, epicardial cells have been identified and used as another important cell type for co-culture with cardiomyocytes to significantly improve cardiomyocyte mechanics and structure. Justification for the co-culture of cardiomyocytes with epicardial cells can be easily explained through the lens of developmental biology. As previously noted, hiPSC-derived cardiomyocytes are immature, resembling the functionality of embryonic cardiomyocytes [171]. During mammalian embryonic development, epicardium-derived cells migrate into the myocardium and contribute to coronary artery development, valve maturation, Purkinje fiber formation and myocardial architecture [234]. *In vitro* studies have shown epicardial-derived cells promote cardiomyocyte proliferation with regulation through retinoic acid and erythropoietin signaling [235] and enhance cardiomyocyte maturation and alignment through direct interaction of epicardial cells with cardiomyocytes [236]. Bargehr et al. used hESC-derived epicardial and cardiomyocytes to augment cardiomyocyte function in 3D engineered cardiac tissues [237]. Structurally, Bargehr et al. observed increased compaction, sarcomere length, cell diameter, cell sectional area, myofibril alignment and expression of connexin 43. Such structural tissue maturity was followed by functional improvements as 3D cardiac tissues supplemented with epicardial cells displayed increased contractility, Frank-Starling relationship, active force production with increasing strain and more mature calcium handling capabilities. Furthermore, the engineered cardiac tissue supplemented with epicardial cells was grafted to the infarcted zone of rat hearts *in vivo*. Although there was no effect on infarct scar, rats treated with the engineered cardiac tissue supplemented with epicardial cells had increased microvasculature, 2.6-fold larger grafts, and improved fractional shortening at 4 weeks.

Although these studies suggest multi-cellular systems can better recapitulate the cellulome of the native heart and thus improve the fidelity of engineered cardiac tissue, such systems are complex. Our understanding of heterotypic cellular interactions in cardiac tissue is not complete and logistical challenges ensue when maintaining and incorporating different cell types in culture. In culturing multi-cellular systems, special attention is required to ensure appropriate cell fractions as cardiomyocytes are non-proliferative and most non-cardiomyocytes, such as fibroblasts, can proliferate, although at different rates in 3D tissues versus sparse 2D culture. Additionally, patterning of different cell types may become necessary. Typically, and in the studies discussed, non-cardiomyocyte cell populations were added to the cell mixture used to form 3D cardiac tissues; however, in order to achieve the physiologically relevant structural organization of multi-cellularity, different cell population may need to be patterned through techniques such as bioprinting or layer-by-layer tissue assembly with different cell geometry and composition in each layer [238].

Hydrogel Formulations: As discussed, hydrogels are often utilized in tissue engineering due to their ability to mimic the native ECM, entrap high concentrations of cells and maintain their shape. A variety of different components are used to create hydrogels for engineering cardiac tissue which include but are not limited to fibrin [239–241], collagen I [209,242,243], Matrigel® [243] and Geltrex™ [209]. Kaiser et al. utilized a design of experiment approach to investigate the relationship between collagen concentration, fibrin concentration, seeding density and cardiomyocyte purity in engineering 3D cardiac tissues [244]. Kaiser et al. reported increased fibrin concentration and seeding density were each associated with increased compaction, while increased collagen concentration was associated with decreased compaction. From this study, the greatest compaction of cardiac tissue was predicted to occur in constructs prepared with a 40–50% cTnT-positive population. Such a study illustrates the need for systematic evaluation of the role of different components in engineering cardiac tissue in order to (1) gain a better mechanistic understanding; (2) optimize cardiac tissue function; and (3) establish standardized, repeatable technologies. Future work utilizing hydrogels in cardiac tissue engineering and better understanding how their components influence cardiac tissue structure, mechanics and function will enhance our understanding of cell-material interactions and ability to engineer cardiomyocyte-based epicardial therapies.

5. New Directions

5.1. Utilizing models

The models used to study MI are extremely important to consider when performing and analyzing potential therapies. Two models of particular relevance are animals and computational simulations.

5.1.1. Animal models

Animal models have often been utilized in researching the cardiovascular system in order to recapitulate its biological complexity. The ideal animal model should resemble the human heart – genetically, biochemically, mechanically, geometrically and hemodynamically. An extensive review detailing the advantages and disadvantages of different animal models in cardiovascular research has been discussed by Milani-Nejad and Janssen [245]. In the context of this discussion, however, some of the mechanical and hemodynamic properties of rat, canine, ovine and porcine animal models will be highlighted.

The cardiac mechanical environment of different animals can vary significantly. As discussed, the passive mechanical properties of the myocardium are largely determined by the titin protein and its isoform. In adult rodents, where the N2B titin isoform dominates, the myocardial has a high passive stiffness. Larger animals and humans, on the other hand, have an increased proportion of the N2BA titin isoform, resulting in more compliant passive myocardium [69,70]. Additionally, two isoforms of the myosin heavy chains (MHC) exist in cardiomyocytes, α-and β-MHC, with the α-MHC isoform having increased ATPase activity and contractile velocity compared to the β-MHC isoform [246]. Human ventricular cardiomyocytes predominately express the β-MHC [247,248]. While larger animals resemble humans in β-MHC expression [245], ventricular cardiomyocyte from small animals, such as rats, predominately express the α-MHC [249].

Hemodynamic levels are comparable between animal models, while heart rate is generally inversely proportional to body weight [245]. Anatomically, swine models feature limited anastomosis in the cardiac coronary arteries, thus resembling a younger human heart, while canine models feature collateralization, thus resembling more of an older human heart [250]. Based on these mechanical and structural differences, post MI outcome can vary. For example, canine models develop dilated cardiomyopathy readily but are less susceptible to myocardial infarction [250]. Additionally, as previously discussed, the anisotropic properties of the healing infarct vary across animal models with rats having isotropic infracts [93] while canine and swine develop anisotropic infarcts [94,95].

5.1.2. Computational models

Recently, computational modeling has been an especially insightful resource in eliciting the mechanical response of the heart to cardiac therapies. The use of such model in a predictive capacity has the advantage of saving time, money and resources as well as allowing for better understanding of the mechanism surrounding the therapeutic treatment. In regard to epicardial restraint therapies, many computational models have been developed to study the functional outcome of specific therapies. For example, Lin et al. utilized finite element analysis to study the functional benefits of a viscoelastic patch on cardiac function post-MI [145]. Additionally, previously discussed models have investigated the impact of anisotropic epicardial restraint on cardiac function [148–150].

Computational modeling has also aided researchers in determining key cellular pathways during MI healing. For example, cardiomyocyte

stretching in the infarcted region is an important consideration when analyzing myocardial function post-MI. Under normal conditions, total tension can be generated from individual cardiomyocytes through isometric (constant length) and isotonic (length change) contraction. However, in the ischemic environment, the cardiomyocytes lose this ability to create tension. Instead, these cells passively stretch, as illustrated in the PV loops mapped by Tyberg et al. [251]. Instead of the counterclockwise cycles seen in healthy myocardium, resulting from the tension developed by the cardiomyocytes, the passive lengthening of the ischemic myocardium results in a clockwise loop. This is an important distinction: instead of the myocardium *performing* the work, the work is being *performed on* the myocardium. Additionally, Tyberg et al. observed hysteresis as the end-diastolic length increased at every end-diastolic pressure, suggesting that the work performed by the surrounding healthy myocardium was being dissipated into the stretching of the ischemic region. Using computation modeling, Tan et al. built a map of 124 interactions of 94 stretch-responsive signaling proteins determined through an extensive literature review. This model illustrates the extensive connection synergy between multiple pathways from cardiomyocyte. Sensitivity testing allowed for the identification of key hubs: calcium, actin, Ras, Raf2, P13k and JAK [252].

5.2. Quantitative restraint

An important consideration when discussing methods to mechanically restrain the heart is how such restraint can be quantified. If successful, restraint devices should limit dilation and reduce the diameter of the heart; this means that restraint over the course of treatment will decline as observed by Ghanta et al. [253].

Researchers have developed epicardial restraint devices with the ability to measure and adjust restraint during therapy. This helps answer questions surrounding the ideal restraint level and the need to maintain it throughout treatment. Ghanta et al. studied immediate (2 months) and long-term (4 months) impact of restraint level (0,3,5 and 8 mmHg) in ovine models using a fluid-filled balled to apply force to the epicardial surface. In this study, 3 mmHg was identified as optimal, although this level was not maintained throughout the experiment [253]. Similarly, Lee et al. also found 3 mmHg to be the ideal level in decreasing LV dilation and improving LV ejection in ovine MI models [254]. Unlike Ghanta et al., Lee et al. maintained the 3 mmHg restraint level by changing the fluid volume within their epicardial patch. Maintenance of this restraint decreased left ventricular end diastolic volume and increased ejection fraction as compared to standard restraint, suggesting a benefit in maintaining a desired restraint level [254].

Another question which arises in regard to restraint quantification is the amount of pre-stretch is necessary at the time of application to the heart. Using computational modeling Lin et al. demonstrated that epicardial therapies with increased stiffness are more sensitive to pre-stretching [145]. It may also be important to consider the impact of general anesthesia on ventricular structure. Using echocardiography, Stein et al. observed differences in structural metrics such as LV end-diastolic diameter and cross-sectional diastolic area when comparing mice samples treated with the anesthetics isoflurane or ketamine/xylazine compared to conscious mice [255].

5.3. Implant timing

As discussed, the healing process after a MI is a dynamic process. The timing at which treatment, whether acellular or cellular, is applied may impact its efficacy. When considering epicardial reinforcement, it seems logical that the therapy would be applied prior to or at the necrotic phase of healing, where the infarct is at highest risk of rupture. For cellular epicardial therapies, however, such timing may also aid in cell retention. For example, Cezar et al. found that when myoblast transplantation was performed during peak inflammation, there was enhanced tissue perfusion, decreased fibrosis and increased contractility [256].

Whyte et al. developed an epicardial device called Therepi, constructed using GelMA and Gelfoam with a subcutaneous port through which cells and other drugs could be administered [257]. Administration of cells over four weeks using Therepi showed improved ejection fraction, fractional shortening and stroke work in MI rat models as compared to single injection of the cells.

5.4. Adding functionality

Although this review focused on the inspiration of cardiac mechanics and structure in developing biomaterial based epicardial restraint devices, there is great potential in engineering such therapies with additional functionality.

5.4.1. Cytokine loading

Local and controlled delivery of cytokines to the infarcted area can be achieved by loading these factors in epicardial restraint therapies. Recently published work in our lab illustrates this technique. Munarin et al. engineered epicardial patches containing hiPSC-derived cardiomyocytes and alginate microspheres loaded with vascular endothelial growth factor (VEGF), basic fibroblast growth factor (bFGF) and sonic hedgehog. *In vivo* implantation showed the angiogenic "cocktail" increased vascularization both in the infarcted area and into the engineered tissue [258]. Release of cytokines by epicardial therapies can also be used to modulate the immune response in the healing myocardium post-MI [259]. Cheng et al. created an acellular epicardial patch made of decellularized porcine myocardium tissue and "synthetic cardiac stromal cells" which were actually biodegradable PLGA microparticles containing three key factors secreted by cardiac stromal cells: VEGF, hepatocyte growth factor (HGF) and insulin-like growth factor (IGF) [260]. This treatment improved left ventricle ejection fraction and fractional shortening in post-MI rats and decreased infarct size while increase infarct wall thickness in porcine post-MI models.

5.4.2. Exosomes

Exosomes are membrane-enclosed vesicles that may carry proteins, mRNAs, microRNAs or additional bioactive material and thus play a key role in cell-cell communication. Recently, exosomes have been identified to play an important role cardiovascular disease, a topic reviewed extensively by Yu and Wang [261]. Recent studies demonstrate the ability of exosomes to induce cardiomyocyte proliferation, promote angiogenesis and modulate cardiomyocyte apoptosis and hypertrophy [262]. Further, exosomes isolated by cardiomyocytes in the infarcted region post-MI have been shown to regulate the local inflammatory response [263]. Through better understanding the role of exosomes, the materials carried by them and their impact in infarct repair, technologies can be developed to mimic exosomes or modulate their activity in order to promote repair in the infarcted myocardium post-MI [262]. Similar to cytokine loading of materials, these identified factors may be used in conjunction with epicardial therapies that provide mechanical support in order to activate intrinsic biochemical healing pathways.

5.4.3. Cell type

Although the cellularized constructs in this review predominately focused on those with contractile cardiomyocytes, application of other cell types to the infarcted myocardium have been shown to improve cardiac function post-MI. This may be in part to a paracrine effect, in which secreted molecules from the implanted cells promote altered remodeling within the infarcted myocardium as opposed to the active contraction which can be achieved utilizing cardiomyocytes.

As previously mentioned, co-culture of cardiomyocytes with endothelial cells [204,209,225–227], human marrow stromal cells [209,226] and pericyte cells [228] promote vascularization. However, utilization of only non-cardiomyocytes has also resulted in improved cardiac function post-MI. For example, Kellar et al. utilized human dermal

fibroblasts in a cardiac patch resulting in higher ejection fraction; however, this was compared only to infarcted mice with no treatment [264]. Additional cell types, such as endothelial and cells and smooth muscle cells in a fibrin matrix [265], adipose-derived stem cells [266] and mesenchymal stem cells in a fibrin patch [241,267], have been used in MI-treatment, all reporting functional benefits.

5.4.4. Electrical integration

Propagation of the electrical signal within the heart is a key element in achieving coordinated contraction. The scar tissue developed after MI is largely non-conductive with fibroblasts able to carry an electrical signal only up to 300 μm [268]. When cellularized patches are applied to the epicardial surface of the heart post-MI, it is extremely important that patch electrically couples with the host in order to avoid potential arrythmia and dysfunction. Gerbin et al. illustrated that cardiomyocyte patch implants on the epicardial surface of rats did not electrically couple to the host after 4 weeks, most likely due to the physical barrier of the scar tissue [269], suggesting the importance of developing techniques to promote electrical integration of epicardial therapies. However, this study demonstrated that intramyocardial hiPSC-derived cardiomyocytes were able to electrically couple to the host rat at heart rates up to 6 Hz, validating the use of the rat as a model for studying electrical coupling of hiPSC-derived cardiomyocyte therapies. One approach to overcome the challenge of epicardial implant coupling is incorporating electrically conductive material that can connect the healthy myocardium with the epicardial therapy. Behabtu et al. developed a wet spinning technique to create macroscopic carbon nanotube fibers, which can be sewn across the epicardial scar and electrically paced [270]. Testing of this design in ovine models showed improve conduction velocity over the scar area [271]. Additionally, Park et al. developed a styrene-butadiene-styrene polymer with silver nanowires mesh. This device not only provided structural reinforcement but increased electrical conduction across the infarcted myocardium [272]. Additionally, electrically conductive scaffolds for cardiac tissue engineering has been an important and innovative field in ensuring proper and mature electrical activity of engineered tissue. A variety of materials such as gold nanoparticles, carbon nanotubes, graphene, polypyrrole and polyaniline have been utilized; these materials and their impact on engineered cardiac tissue is reviewed in great detail by Baei et al. [273].

6. Conclusion

The cardiac mechanostructure plays a key role in physiological function and pathological dysfunction of the heart. The helical organization of myocardial fibers within the ventricular wall, coupled with their active contraction, are responsible for the twisting motion and subsequent functional efficiency of the heart. MI significantly disrupts the mechanics and structure of the heart. From the death of actively contracting cardiomyocytes to compositional changes in the deposited ECM, the myocardium must adjust to this new environment, often time undergoing significant remodeling in order to preserve cardiac output. Epicardial therapies aim to limit deleterious ventricular remodeling and its progression into HF.

Many epicardial therapies are being developed to recapitulate the mechanical and structural properties of the healthy myocardium and address the functional loss induced by MI. These therapies, which encompass passive and active devices, are promising alternatives to current treatments, such as LVADs and heart transplantation, and address an unmet need for patients unresponsive to conventional drug therapies on a trajectory towards HF. Further research into the fundamental knowledge surrounding MI changes in the myocardial environment as well as interdisciplinary cooperation is necessary for continued development of epicardial therapies for treating post-MI heart regeneration.

CRediT authorship contribution statement

Kiera D. Dwyer: Conceptualization, Writing - original draft, Review & Editing. **Kareen L.K. Coulombe:** Conceptualization, Writing - review & editing, Funding acquisition.

Declaration of competing interest

The authors have no conflicts of interest to declare.

Acknowledgemwnts

We gratefully acknowledge funding from the National Institutes of Health, National Heart, Lung, and Blood Institute grant number R01 HL135091.

References

[1] H.N. Sabbah, The cardiac support device and the Myosplint: treating heart failure by targeting left ventricular size and shape, Ann. Thorac. Surg. 75 (6) (2003) S13–S19.
[2] N.J. Kaiser, J.A. Bellows, R.J. Kant, K.L.K. Coulombe, Digital design and automated fabrication of bespoke collagen microfiber scaffolds, Tissue Eng. C Methods (2019).
[3] E.J. Benjamin, S.S. Virani, C.W. Callaway, A.M. Chamberlain, A.R. Chang, S. Cheng, S.E. Chiuve, M. Cushman, F.N. Delling, R. Deo, Heart disease and stroke statistics—2018 update: a report from the American Heart Association, Circulation, 2018.
[4] T.J. Cahill, R.K. Kharbanda, Heart failure after myocardial infarction in the era of primary percutaneous coronary intervention: mechanisms, incidence and identification of patients at risk, World J. Cardiol. 9 (5) (2017) 407–415.
[5] W.-N. Lu, S.-H. Lü, H.-B. Wang, D.-X. Li, C.-M. Duan, Z.-Q. Liu, T. Hao, W.-J. He, B. Xu, Q. Fu, Y.C. Song, X.-H. Xie, C.-Y. Wang, Functional improvement of infarcted heart by Co-injection of embryonic stem cells with temperature-responsive chitosan hydrogel, Tissue Eng. 15 (6) (2008) 1437–1447.
[6] A. D'Amore, T. Yoshizumi, S.K. Luketich, M.T. Wolf, X. Gu, M. Cammarata, R. Hoff, S.F. Badylak, W.R. Wagner, Bi-layered polyurethane - extracellular matrix cardiac patch improves ischemic ventricular wall remodeling in a rat model, Biomaterials 107 (2016) 1–14.
[7] E.T. Roche, M.A. Horvath, I. Wamala, A. Alazmani, S.-E. Song, W. Whyte, Z. Machaidze, C.J. Payne, J.C. Weaver, G. Fishbein, J. Kuebler, N.V. Vasilyev, D. J. Mooney, F.A. Pigula, C.J. Walsh, Soft robotic sleeve supports heart function, Sci. Transl. Med. 9 (373) (2017), eaaf3925.
[8] J.J. Song, H.C. Ott, Organ engineering based on decellularized matrix scaffolds, Trends Mol. Med. 17 (8) (2011) 424–432.
[9] W. Bian, N. Badie, H.D. Himel, N. Bursac, Robust T-tubulation and maturation of cardiomyocytes using tissue-engineered epicardial mimetics, Biomaterials 35 (12) (2014) 3819–3828.
[10] C. Holubarsch, T. Ruf, J. Goldstein Daniel, C. Ashton Robert, W. Nickl, B. Pieske, K. Pioch, J. Lüdemann, S. Wiesner, G. Hasenfuss, H. Posival, H.r. Just, D. Burkhoff, Existence of the frank-starling mechanism in the failing human heart, Circulation 94 (4) (1996) 683–689.
[11] S. Nakatani, Left ventricular rotation and twist: why should we learn? Journal of cardiovascular ultrasound 19 (1) (2011) 1–6.
[12] G.D. Buckberg, H.C. Coghlan, J.I.E. Hoffman, F. Torrent-Guasp, The structure and function of the helical heart and its buttress wrapping. VII. Critical importance of septum for right ventricular function, Semin. Thorac. Cardiovasc. Surg. 13 (4) (2001) 402–416.
[13] G.D. Buckberg, Basic science review: the helix and the heart, J. Thorac. Cardiovasc. Surg. 124 (5) (2002) 863–883.
[14] E.A. Sallin, Fiber orientation and ejection fraction in the human left ventricle, Biophys. J. vol. 9 (7) (1969) 954–964.
[15] R. Rehman, V.S. Yelamanchili, A.N. Makaryus, cardiac imaging, in: *StatPearls*. Treasure Island (FL), 2020.
[16] E. Cutrì, M. Serrani, P. Bagnoli, R. Fumero, M.L. Costantino, The cardiac torsion as a sensitive index of heart pathology: a model study, Journal of the Mechanical Behavior of Biomedical Materials 55 (2016) 104–119.
[17] H.-S. Ahn, Y.-K. Kim, H.C. Song, E.J. Choi, G.-H. Kim, J.S. Cho, S.-H. Ihm, H.-Y. Kim, C.S. Park, H.-J. Youn, The impact of preload on 3-dimensional deformation parameters: principal strain, twist and torsion, Cardiovasc. Ultrasound 15 (1) (2017) 22.
[18] J.-z. Xia, J.-y. Xia, G. Li, W.-y. Ma, Q.-q. Wang, Left ventricular strain examination of different aged adults with 3D speckle tracking echocardiography, Echocardiography 31 (3) (2014) 335–339.
[19] C.C. Moore, E.R. McVeigh, E.A. Zerhouni, Quantitative tagged magnetic resonance imaging of the normal human left ventricle, Top. Magn. Reson. Imag. : TMRI 11 (6) (2000) 359–371.
[20] A.H. Soepriatna, A.K. Yeh, A.D. Clifford, S.E. Bezci, G.D. O'Connell, C.J. Goergen, Three-dimensional myocardial strain correlates with murine left ventricular remodelling severity post-infarction, J. R. Soc. Interface 16 (160) (2019) 20190570.

[21] S. Nielles-Vallespin, Z. Khalique, P.F. Ferreira, R. de Silva, A.D. Scott, P. Kilner, L.-A. McGill, A. Giannakidis, P.D. Gatehouse, D. Ennis, E. Aliotta, M. Al-Khalil, P. Kellman, D. Mazilu, R.S. Balaban, D.N. Firmin, A.E. Arai, D.J. Pennell, Assessment of myocardial microstructural dynamics by in vivo diffusion tensor cardiac magnetic resonance, J. Am. Coll. Cardiol. 69 (6) (2017) 661.
[22] M.-T. Wu, W.-Y. Tseng, M.-Y. Su, C.-P. Liu, K.-R. Chiou, V.J. Wedeen, T.G. Reese, C.-F. Yang, Diffusion tensor magnetic resonance imaging mapping the fiber architecture remodeling in human myocardium after infarction: correlation with viability and wall motion, Circulation 114 (10) (2006) 1036–1045.
[23] S. Zhang, J.A. Crow, X. Yang, J. Chen, A. Borazjani, K.B. Mullins, W. Chen, R. C. Cooper, R.M. McLaughlin, J. Liao, The correlation of 3D DT-MRI fiber disruption with structural and mechanical degeneration in porcine myocardium, Ann. Biomed. Eng. 38 (10) (2010) 3084–3095.
[24] C. Papadacci, V. Finel, J. Provost, O. Villemain, P. Bruneval, J.-L. Gennisson, M. Tanter, M. Fink, M. Pernot, Imaging the dynamics of cardiac fiber orientation in vivo using 3D Ultrasound Backscatter Tensor Imaging, Sci. Rep. 7 (1) (2017) 830.
[25] S.J. Shah, B.A. Borlaug, D.W. Kitzman, A.D. McCulloch, B.C. Blaxall, R. Agarwal, J.A. Chirinos, S. Collins, R.C. Deo, M.T. Gladwin, H. Granzier, S.L. Hummel, D. A. Kass, M.M. Redfield, F. Sam, T.J. Wang, P. Desvigne-Nickens, B.B. Adhikari, Research priorities for heart failure with preserved ejection fraction, Circulation 141 (12) (2020) 1001–1026.
[26] A.P. Voorhees, H.-C. Han, Biomechanics of cardiac function, Comprehensive Physiology 5 (4) (2015) 1623–1644.
[27] W. Grossman, W.J. Paulus, Myocardial stress and hypertrophy: a complex interface between biophysics and cardiac remodeling, J. Clin. Invest. 123 (9) (2013) 3701–3703.
[28] H. Kögler, P. Schott, K. Toischer, H. Milting, P.N. Van, M. Kohlhaas, C. Grebe, A. Kassner, E. Domeier, N. Teucher, T. Seidler, R. Knöll, L.S. Maier, A. El-Banayosy, R. Körfer, G. Hasenfuss, Relevance of brain natriuretic peptide in preload-dependent regulation of cardiac sarcoplasmic reticulum Ca2+ ATPase expression, Circulation 113 (23) (2006) 2724–2732.
[29] K. Toischer, H. Kögler, G. Tenderich, C. Grebe, T. Seidler, P.N. Van, K. Jung, R. Knöll, R. Körfer, G. Hasenfuss, Elevated afterload, neuroendocrine stimulation, and human heart failure increase BNP levels and inhibit preload-dependent SERCA upregulation, Circ Heart Fail 1 (4) (2008) 265–271.
[30] K. Toischer, A.G. Rokita, B. Unsöld, W. Zhu, G. Kararigas, S. Sossalla, S.P. Reuter, A. Becker, N. Teucher, T. Seidler, C. Grebe, L. Preuss, S.N. Gupta, K. Schmidt, S. E. Lehnart, M. Krüger, W.A. Linke, J. Backs, V. Regitz-Zagrosek, K. Schäfer, L. J. Field, L.S. Maier, G. Hasenfuss, Differential cardiac remodeling in preload versus afterload, Circulation 122 (10) (2010) 993–1003.
[31] K. Ronaldson-Bouchard, K. Yeager, D. Teles, T. Chen, S. Ma, L. Song, K. Morikawa, H.M. Wobma, A. Vasciaveo, E.C. Ruiz, M. Yazawa, G. Vunjak-Novakovic, Engineering of human cardiac muscle electromechanically matured to an adult-like phenotype, Nat. Protoc. 14 (10) (2019) 2781–2817.
[32] R. Ng, L.R. Sewanan, A.L. Brill, P. Stankey, X. Li, Y. Qyang, B.E. Ehrlich, S. G. Campbell, Contractile work directly modulates mitochondrial protein levels in human engineered heart tissues, Am. J. Physiol. Heart Circ. Physiol. 318 (6) (2020) H1516–H1524.
[33] A. Leonard, A. Bertero, J.D. Powers, K.M. Beussman, S. Bhandari, M. Regnier, C. E. Murry, N.J. Sniadecki, Afterload promotes maturation of human induced pluripotent stem cell derived cardiomyocytes in engineered heart tissues, J. Mol. Cell. Cardiol. 118 (2018) 147–158.
[34] T. Boudou, W.R. Legant, A. Mu, M.A. Borochin, N. Thavandiran, M. Radisic, P. W. Zandstra, J.A. Epstein, K.B. Margulies, C.S. Chen, A microfabricated platform to measure and manipulate the mechanics of engineered cardiac microtissues, Tissue Eng. 18 (9–10) (2012) 910–919.
[35] M.N. Hirt, N.A. Sörensen, L.M. Bartholdt, J. Boeddinghaus, S. Schaaf, A. Eder, I. Vollert, A. Stöhr, T. Schulze, A. Witten, M. Stoll, A. Hansen, T. Eschenhagen, Increased afterload induces pathological cardiac hypertrophy: a new in vitro model, Basic Res. Cardiol. 107 (6) (2012), 307-307.
[36] X. Shi, Y. Liu, K.M. Copeland, S.R. McMahan, S. Zhang, J.R. Butler, Y. Hong, M. Cho, P. Bajona, H. Gao, J. Liao, Epicardial prestrained confinement and residual stresses: a newly observed heart ventricle confinement interface, J. R. Soc. Interface 16 (152) (2019) 20190028.
[37] P.D. Jöbsis, H. Ashikaga, H. Wen, E.C. Rothstein, K.A. Horvath, E.R. McVeigh, R. S. Balaban, The visceral pericardium: macromolecular structure and contribution to passive mechanical properties of the left ventricle, Am. J. Physiol. Heart Circ. Physiol. 293 (6) (2007) H3379–H3387.
[38] G.M. Fomovsky, S. Thomopoulos, J.W. Holmes, Contribution of extracellular matrix to the mechanical properties of the heart, J. Mol. Cell. Cardiol. 48 (3) (2010) 490–496.
[39] M.J. Kocica, A.F. Corno, V. Lackovic, V.I. Kanjuh, The helical ventricular myocardial band of torrent-guasp, Semin. Thorac. Cardiovasc. Surg. Pediatr. Card Surg. Annu. 10 (1) (2007) 52–60.
[40] C. Papadacci, V. Finel, J. Provost, O. Villemain, P. Bruneval, J.L. Gennisson, M. Tanter, M. Fink, M. Pernot, Imaging the dynamics of cardiac fiber orientation in vivo using 3D Ultrasound Backscatter Tensor Imaging, Sci. Rep. 7 (1) (2017) 830.
[41] E.R. Pfeiffer, J.R. Tangney, J.H. Omens, A.D. McCulloch, Biomechanics of cardiac electromechanical coupling and mechanoelectric feedback, J. Biomech. Eng. 136 (2) (2014), 021007-21007.
[42] S. Omar Alaa Mabrouk, S. Vallabhajosyula, P. Sengupta Partho, Left ventricular twist and torsion, Circulation: Cardiovascular Imaging 8 (6) (2015), e003029.
[43] P.P. Sengupta, A.J. Tajik, K. Chandrasekaran, B.K. Khandheria, Twist mechanics of the left ventricle, JACC: Cardiovascular Imaging 1 (3) (2008) 366.
[44] Y. Zhang, Q.-c. Zhou, D.-r. Pu, L. Zou, Y. Tan, Differences in left ventricular twist related to age: speckle tracking echocardiographic data for healthy volunteers from neonate to age 70 years, Echocardiography 27 (10) (2010) 1205–1210.
[45] Y. Nagata, V.C.-C. Wu, Y. Otsuji, M. Takeuchi, Normal range of myocardial layer-specific strain using two-dimensional speckle tracking echocardiography, PloS One 12 (6) (2017) e0180584-e0180584.
[46] M.A. Bray, S.P. Sheehy, K.K. Parker, Sarcomere alignment is regulated by myocyte shape, Cell Motil Cytoskeleton 65 (8) (2008) 641–651.
[47] M.J. Kocica, A.F. Corno, F. Carreras-Costa, M. Ballester-Rodes, M.C. Moghbel, C. N.C. Cueva, V. Lackovic, V.I. Kanjuh, F. Torrent-Guasp, The helical ventricular myocardial band: global, three-dimensional, functional architecture of the ventricular myocardium, Eur. J. Cardio. Thorac. Surg. 29 (Supplement_1) (2006) S21–S40.
[48] A.W. Feinberg, P.W. Alford, H. Jin, C.M. Ripplinger, A.A. Werdich, S.P. Sheehy, A. Grosberg, K.K. Parker, Controlling the contractile strength of engineered cardiac muscle by hierarchal tissue architecture, Biomaterials 33 (23) (2012) 5732–5741.
[49] M. Valderrábano, Influence of anisotropic conduction properties in the propagation of the cardiac action potential, Prog. Biophys. Mol. Biol. 94 (1–2) (2007) 144–168.
[50] N. Bursac, K.K. Parker, S. Iravanian, L. Tung, Cardiomyocyte cultures with controlled macroscopic anisotropy: a model for functional electrophysiological studies of cardiac muscle, Circ. Res. 91 (12) (2002) e45–54.
[51] S.W. Patterson, E.H. Starling, On the mechanical factors which determine the output of the ventricles, J. Physiol. 48 (5) (1914) 357–379.
[52] J.R. Basford, The Law of Laplace and its relevance to contemporary medicine and rehabilitation, Arch. Phys. Med. Rehabil. 83 (8) (2002) 1165–1170.
[53] H.C. Oxenham, A.A. Young, B.R. Cowan, T.L. Gentles, C.J. Occleshaw, C. G. Fonseca, R.N. Doughty, N. Sharpe, Age-related changes in myocardial relaxation using three-dimensional tagged magnetic resonance imaging: structure and function, J. Cardiovasc. Magn. Reson. 5 (3) (2003) 421–430.
[54] E.D. Carruth, I. Teh, J.E. Schneider, A.D. McCulloch, J.H. Omens, L.R. Frank, Regional variations in ex-vivo diffusion tensor anisotropy are associated with cardiomyocyte remodeling in rats after left ventricular pressure overload, J. Cardiovasc. Magn. Reson. 22 (1) (2020).
[55] P. Haynes, K.E. Nava, B.A. Lawson, C.S. Chung, M.I. Mitov, S.G. Campbell, A. J. Stromberg, S. Sadayappan, M.R. Bonnell, C.W. Hoopes, K.S. Campbell, Transmural heterogeneity of cellular level power output is reduced in human heart failure, J. Mol. Cell. Cardiol. 72 (2014) 1–8.
[56] J.W. Holmes, T.K. Borg, J.W. Covell, Structure and mechanics of healing myocardial infarcts, Annu. Rev. Biomed. Eng. 7 (1) (2005) 223–253.
[57] A.J. Engler, C. Carag-Krieger, C.P. Johnson, M. Raab, H.-Y. Tang, D.W. Speicher, J.W. Sanger, J.M. Sanger, D.E. Discher, Embryonic cardiomyocytes beat best on a matrix with heart-like elasticity: scar-like rigidity inhibits beating, J. Cell Sci. 121 (22) (2008) 3794–3802.
[58] J.G. Jacot, A.D. McCulloch, J.H. Omens, Substrate stiffness affects the functional maturation of neonatal rat ventricular myocytes, Biophys. J. 95 (7) (2008) 3479–3487.
[59] D.T. Nguyen, N. Nagarajan, P. Zorlutuna, Effect of substrate stiffness on mechanical coupling and force propagation at the infarct boundary, Biophys. J. 115 (10) (2018) 1966–1980.
[60] M.L. McCain, H. Yuan, F.S. Pasqualini, P.H. Campbell, K.K. Parker, Matrix elasticity regulates the optimal cardiac myocyte shape for contractility, Am. J. Physiol. Heart Circ. Physiol. 306 (11) (2014) H1525–H1539.
[61] R. Tennant, C.J. Wiggers, The effect of coronary occlusion on myocardial contraction, American Journal of Physiology-Legacy Content 112 (2) (1935) 351–361.
[62] H.L. Granzier, T.C. Irving, Passive tension in cardiac muscle: contribution of collagen, titin, microtubules, and intermediate filaments, Biophys. J. 68 (3) (1995) 1027–1044.
[63] R.J. Zaunbrecher, A.N. Abel, K. Beussman, A. Leonard, M. von Frieling-Salewsky, P.A. Fields, L. Pabon, H. Reinecke, X. Yang, J. Macadangdang, D.H. Kim, W. A. Linke, N.J. Sniadecki, M. Regnier, C.E. Murry, Cronos titin is expressed in human cardiomyocytes and necessary for normal sarcomere function, Circulation 140 (20) (2019) 1647–1660.
[64] R. Yamasaki, Y. Wu, M. McNabb, M. Greaser, S. Labeit, H. Granzier, Protein kinase A phosphorylates titin's cardiac-specific N2B domain and reduces passive tension in rat cardiac myocytes, Circ. Res. 90 (11) (2002) 1181–1188.
[65] M. Krüger, S. Kötter, A. Grützner, P. Lang, C. Andresen, M.M. Redfield, E. Butt, C. G. dos Remedios, W.A. Linke, Protein kinase G modulates human myocardial passive stiffness by phosphorylation of the titin springs, Circ. Res. 104 (1) (2009) 87–94.
[66] A. Grützner, S. Garcia-Manyes, S. Kötter, C.L. Badilla, J.M. Fernandez, W. A. Linke, Modulation of titin-based stiffness by disulfide bonding in the cardiac titin N2-B unique sequence, Biophys. J. 97 (3) (2009) 825–834.
[67] H. Fujita, D. Labeit, B. Gerull, S. Labeit, H.L. Granzier, Titin isoform-dependent effect of calcium on passive myocardial tension, Am. J. Physiol. Heart Circ. Physiol. 287 (6) (2004) H2528–H2534.
[68] D. Labeit, K. Watanabe, C. Witt, H. Fujita, Y. Wu, S. Lahmers, T. Funck, S. Labeit, H. Granzier, Calcium-dependent molecular spring elements in the giant protein titin, Proc. Natl. Acad. Sci. U. S. A. 100 (23) (2003) 13716–13721.
[69] K. Trombitás, A. Redkar, T. Centner, Y. Wu, S. Labeit, H. Granzier, Extensibility of isoforms of cardiac titin: variation in contour length of molecular subsegments provides a basis for cellular passive stiffness diversity, Biophys. J. 79 (6) (2000) 3226–3234.

[70] M.M. LeWinter, H. Granzier, Cardiac titin: a multifunctional giant, Circulation 121 (19) (2010) 2137–2145.
[71] J. Lin, Y. Shi, Y. Men, X. Wang, J. Ye, C. Zhang, Mechanical roles in formation of oriented collagen fibers, Tissue Eng. B Rev. 26 (2) (2019) 116–128.
[72] J.K. Mouw, G. Ou, V.M. Weaver, Extracellular matrix assembly: a multiscale deconstruction, Nat. Rev. Mol. Cell Biol. 15 (12) (2014) 771–785.
[73] M.D. Shoulders, R.T. Raines, Collagen structure and stability, Annu. Rev. Biochem. vol. 78 (2009) 929–958.
[74] M. Marino, G. Vairo, Multiscale elastic models of collagen bio-structures: from cross-linked molecules to soft tissues, in: Multiscale Computer Modeling in Biomechanics and Biomedical Engineering, Springer, 2013, pp. 73–102.
[75] G. Kenneth Mallory, P.D. White, J. Salcedo-Salgar, The speed of healing of myocardial infarction: a study of the pathologic anatomy in seventy-two cases, Am. Heart J. 18 (6) (1939) 647–671.
[76] M.C. Fishbein, D. Maclean, P.R. Maroko, The histopathologic evolution of myocardial infarction, Chest 73 (6) (1978) 843–849.
[77] W. Phatharajaree, A. Phrommintikul, N. Chattipakorn, Matrix metalloproteinases and myocardial infarction, Can. J. Cardiol. 23 (9) (2007) 727–733.
[78] E. Herzog, A. Gu, T. Kohmoto, D. Burkhoff, J.S. Hochman, Early activation of metalloproteinases after experimental myocardial infarction occurs in infarct and non-infarct zones, Cardiovasc. Pathol. 7 (6) (1998) 307–312.
[79] J.P. Cleutjens, J.C. Kandala, E. Guarda, R.V. Guntaka, K.T. Weber, Regulation of collagen degradation in the rat myocardium after infarction, J. Mol. Cell. Cardiol. 27 (6) (1995) 1281–1292.
[80] Y. Birnbaum, A.J. Chamoun, A. Anzuini, S.D. Lick, M. Ahmad, B.F. Uretsky, Ventricular free wall rupture following acute myocardial infarction, Coron. Artery Dis. 14 (6) (2003) 463–470.
[81] L.R. Sewanan, J. Schwan, J. Kluger, J. Park, D.L. Jacoby, Y. Qyang, S. G. Campbell, Extracellular matrix from hypertrophic myocardium provokes impaired twitch dynamics in healthy cardiomyocytes, JACC: Basic to Translational Science 4 (4) (2019) 495–505.
[82] M.F. Berry, A.J. Engler, Y.J. Woo, T.J. Pirolli, L.T. Bish, V. Jayasankar, K. J. Morine, T.J. Gardner, D.E. Discher, H.L. Sweeney, Mesenchymal stem cell injection after myocardial infarction improves myocardial compliance, Am. J. Physiol. Heart Circ. Physiol. 290 (6) (2006) H2196–H2203.
[83] E.A. Corbin, A. Vite, E.G. Peyster, M. Bhoopalam, J. Brandimarto, X. Wang, A. I. Bennett, A.T. Clark, X. Cheng, K.T. Turner, K. Musunuru, K.B. Margulies, Tunable and reversible substrate stiffness reveals a dynamic mechanosensitivity of cardiomyocytes, ACS Appl. Mater. Interfaces 11 (23) (2019) 20603–20614.
[84] K.E. Sullivan, K.P. Quinn, K.M. Tang, I. Georgakoudi, L.D. Black, Extracellular matrix remodeling following myocardial infarction influences the therapeutic potential of mesenchymal stem cells, Stem Cell Res. Ther. 5 (1) (2014) 14.
[85] A. Kruzynska-Frejtag, M. Machnicki, R. Rogers, R.R. Markwald, S.J. Conway, Periostin (an osteoblast-specific factor) is expressed within the embryonic mouse heart during valve formation, Mech. Dev. 103 (1–2) (2001) 183–188.
[86] R.A. Norris, B. Damon, V. Mironov, V. Kasyanov, A. Ramamurthi, R. Moreno-Rodriguez, T. Trusk, J.D. Potts, R.L. Goodwin, J. Davis, S. Hoffman, X. Wen, Y. Sugi, C.B. Kern, C.H. Mjaatvedt, D.K. Turner, T. Oka, S.J. Conway, J. D. Molkentin, G. Forgacs, R.R. Markwald, Periostin regulates collagen fibrillogenesis and the biomechanical properties of connective tissues, J. Cell. Biochem. 101 (3) (2007) 695–711.
[87] M. Shimazaki, K. Nakamura, I. Kii, T. Kashima, N. Amizuka, M. Li, M. Saito, K. Fukuda, T. Nishiyama, S. Kitajima, Y. Saga, M. Fukayama, M. Sata, A. Kudo, Periostin is essential for cardiac healingafter acute myocardial infarction, J. Exp. Med. 205 (2) (2008) 295–303.
[88] D.R. Keene, E. Engvall, R.W. Glanville, Ultrastructure of type VI collagen in human skin and cartilage suggests an anchoring function for this filamentous network, Journal of Cell Biology 107 (5) (1988) 1995–2006.
[89] J. Luther Daniel, K. Thodeti Charles, E. Shamhart Patricia, K. Adapala Ravi, C. Hodnichak, D. Weihrauch, P. Bonaldo, M. Chilian William, J.G. Meszaros, Absence of type VI collagen paradoxically improves cardiac function, structure, and remodeling after myocardial infarction, Circ. Res. 110 (6) (2012) 851–856.
[90] K. Rasi, J. Piuhola, M. Czabanka, R. Sormunen, M. Ilves, H. Leskinen, J. Rysä, R. Kerkelä, P. Janmey, R. Heljasvaara, K. Peuhkurinen, O. Vuolteenaho, H. Ruskoaho, P. Vajkoczy, T. Pihlajaniemi, L. Eklund, Collagen XV is necessary for modeling of the extracellular matrix and its deficiency predisposes to cardiomyopathy, Circ. Res. 107 (10) (2010) 1241–1252.
[91] L. Eklund, J. Piuhola, J. Komulainen, R. Sormunen, C. Ongvarrasopone, R. Fässler, A. Muona, M. Ilves, H. Ruskoaho, T.E.S. Takala, T. Pihlajaniemi, Lack of type XV collagen causes a skeletal myopathy and cardiovascular defects in mice, Proc. Natl. Acad. Sci. Unit. States Am. 98 (3) (2001) 1194.
[92] J. Atance, M.J. Yost, W. Carver, Influence of the extracellular matrix on the regulation of cardiac fibroblast behavior by mechanical stretch, J. Cell. Physiol. 200 (3) (2004) 377–386.
[93] G.M. Fomovsky, J.W. Holmes, Evolution of scar structure, mechanics, and ventricular function after myocardial infarction in the rat, Am. J. Physiol. Heart Circ. Physiol. 298 (1) (2009) H221–H228.
[94] P. Whittaker, D.R. Boughner, R.A. Kloner, Analysis of healing after myocardial infarction using polarized light microscopy, Am. J. Pathol. 134 (4) (1989) 879–893.
[95] J.W. Holmes, J.A. Nunez, J.W. Covell, Functional implications of myocardial scar structure, Am. J. Physiol. Heart Circ. Physiol. 272 (5) (1997) H2123–H2130.
[96] L.R. Caggiano, J.J. Lee, J.W. Holmes, Surgical reinforcement alters collagen alignment and turnover in healing myocardial infarcts, Am. J. Physiol. Heart Circ. Physiol. 315 (4) (2018) H1041–H1050.
[97] G.M. Fomovsky, A.D. Rouillard, J.W. Holmes, Regional mechanics determine collagen fiber structure in healing myocardial infarcts, J. Mol. Cell. Cardiol. 52 (5) (2012) 1083–1090.
[98] W.S. Haston, J.M. Shields, P.C. Wilkinson, The orientation of fibroblasts and neutrophils on elastic substrata, Experimental Cell Research vol. 146 (1) (1983) 117–126.
[99] E. Marcelli, L. Cercenelli, M. Musaico, P. Bagnoli, M.L. Costantino, R. Fumero, G. Plicchi, Assessment of cardiac rotation by means of gyroscopic sensors, in: Paper Presented at the 2008 Computers in Cardiology, 2008, pp. 14–17.
[100] I. Jugdutt Bodh, W.M. Amy Roger, Healing after myocardial infarction in the dog: changes in infarct hydroxyproline and topography, J. Am. Coll. Cardiol. 7 (1) (1986) 91–102.
[101] M.T. Vivaldi, D.R. Eyre, R.A. Kloner, F.J. Schoen, Effects of methylprednisolone on collagen biosynthesis in healing acute myocardial infarction, Am. J. Cardiol. 60 (4) (1987) 424–425.
[102] C.Y. Choong, E.F. Gibbons, R.D. Hogan, T.D. Franklin, M. Nolting, D.L. Mann, A. E. Weyman, Relationship of functional recovery to scar contraction after myocardial infarction in the canine left ventricle, Am. Heart J. 117 (4) (1989) 819–829.
[103] W.J. Richardson, S.A. Clarke, T.A. Quinn, J.W. Holmes, Physiological implications of myocardial scar structure, Comprehensive Physiology 5 (4) (2015) 1877–1909.
[104] S. Ørn, C. Manhenke, I.S. Anand, I. Squire, E. Nagel, T. Edvardsen, K. Dickstein, Effect of left ventricular scar size, location, and transmurality on left ventricular remodeling with healed myocardial infarction, Am. J. Cardiol. 99 (8) (2007) 1109–1114.
[105] D. Mathey, W. Biefield, P. Hanrath, S. Effert, Attempt to quantitate relation between cardiac function and infarct size in acute myocardial infarction, Br. Heart J. 36 (3) (1974) 271.
[106] P.J. Fletcher, J.M. Pfeffer, M.A. Pfeffer, E. Braunwald, Left ventricular diastolic pressure-volume relations in rats with healed myocardial infarction. Effects on systolic function, Circ. Res. 49 (3) (1981) 618–626.
[107] S.D. Roes, S. Kelle, T.A. Kaandorp, T. Kokocinski, D. Poldermans, H.J. Lamb, E. Boersma, E.E. van der Wall, E. Fleck, A. de Roos, E. Nagel, J.J. Bax, Comparison of myocardial infarct size assessed with contrast-enhanced magnetic resonance imaging and left ventricular function and volumes to predict mortality in patients with healed myocardial infarction, Am. J. Cardiol. 100 (6) (2007) 930–936.
[108] E.H. Schuster, B.H. Bulkley, Expansion of transmural myocardial infarction: a pathophysiologic factor in cardiac rupture, Circulation 60 (7) (1979) 1532–1538.
[109] G.M. Fomovsky, J.W. Holmes, Evolution of scar structure, mechanics, and ventricular function after myocardial infarction in the rat, Am. J. Physiol. Heart Circ. Physiol. 298 (1) (2010) H221–H228.
[110] S.L. Rutherford, M.L. Trew, G.B. Sands, I.J. LeGrice, B.H. Smaill, High-resolution 3-dimensional reconstruction of the infarct border zone: impact of structural remodeling on electrical activation, Circ. Res. 111 (3) (2012) 301–311.
[111] G.K. Yankey, T. Li, A. Kilic, G. Cheng, A. Satpute, K. Savai, S. Li, S.L. Moainie, D. Prastein, C. DeFillipi, Z.J. Wu, B.P. Griffith, Regional remodeling strain and its association with myocardial apoptosis after myocardial infarction in an ovine model, J. Thorac. Cardiovasc. Surg. 135 (5) (2008) 991–998, e992.
[112] I. Gavras, H. Gavras, Angiotensin II as a cardiovascular risk factor, J. Hum. Hypertens. 16 (2) (2002) S2–S6.
[113] J. Müller-Ehmsen, P. Whittaker, R.A. Kloner, J.S. Dow, T. Sakoda, T.I. Long, P. W. Laird, L. Kedes, Survival and development of neonatal rat cardiomyocytes transplanted into adult myocardium, J. Mol. Cell. Cardiol. 34 (2) (2002) 107–116.
[114] E. Tous, B. Purcell, J.L. Ifkovits, J.A. Burdick, Injectable Acellular hydrogels for cardiac repair, Journal of Cardiovascular Translational Research 4 (5) (2011) 528–542.
[115] S.T. Wall, J.C. Walker, K.E. Healy, M.B. Ratcliffe, J.M. Guccione, Theoretical impact of the injection of material into the myocardium: a finite element model simulation, Circulation 114 (24) (2006) 2627–2635.
[116] W. Dai, L.E. Wold, J.S. Dow, R.A. Kloner, Thickening of the infarcted wall by collagen injection improves left ventricular function in rats, J. Am. Coll. Cardiol. 46 (4) (2005) 714.
[117] K.L. Christman, H.H. Fok, R.E. Sievers, Q. Fang, R.J. Lee, Fibrin glue alone and skeletal myoblasts in a fibrin scaffold preserve cardiac function after myocardial infarction, Tissue Eng. 10 (3–4) (2004) 403–409.
[118] K.L. Christman, A.J. Vardanian, Q. Fang, R.E. Sievers, H.H. Fok, R.J. Lee, Injectable fibrin scaffold improves cell transplant survival, reduces infarct expansion, and induces neovasculature formation in ischemic myocardium, J. Am. Coll. Cardiol. 44 (3) (2004) 654.
[119] J.M. Singelyn, J.A. DeQuach, S.B. Seif-Naraghi, R.B. Littlefield, P.J. Schup-Magoffin, K.L. Christman, Naturally derived myocardial matrix as an injectable scaffold for cardiac tissue engineering, Biomaterials 30 (29) (2009) 5409–5416.
[120] M.T. Spang, T.S. Lazerson, S. Bhatia, J. Corbitt, G. Sandoval, C. Luo, K.G. Osborn, P. Cabrales, E. Kwon, F. Contijoch, R.R. Reeves, A.N. DeMaria, K.L. Christman, A New Form of Decellularized Extracellular Matrix Hydrogel for Treating Ischemic Tissue via Intravascular Infusion, 2020, bioRxiv vol. 2004 (2020), 2010.028076.
[121] J.H. Traverse, T.D. Henry, N. Dib, A.N. Patel, C. Pepine, G.L. Schaer, J. A. Dequach, A.M. Kinsey, P. Chamberlin, K.L. Christman, First-in-Man study of a cardiac extracellular matrix hydrogel in early and late myocardial infarction patients, JACC: Basic to Translational Science 4 (6) (2019) 659–669.
[122] N. Landa, L. Miller, M.S. Feinberg, R. Holbova, M. Shachar, I. Freeman, S. Cohen, J. Leor, Effect of injectable alginate implant on cardiac remodeling and function after recent and old infarcts in rat, Circulation 117 (11) (2008) 1388.

[123] O. Tsur-Gang, E. Ruvinov, N. Landa, R. Holbova, M.S. Feinberg, J. Leor, S. Cohen, The effects of peptide-based modification of alginate on left ventricular remodeling and function after myocardial infarction, Biomaterials 30 (2) (2009) 189–195.
[124] T. Wang, D.-Q. Wu, X.-J. Jiang, X.-Z. Zhang, X.-Y. Li, J.-F. Zhang, Z.-B. Zheng, R. Zhuo, H. Jiang, C. Huang, Novel thermosensitive hydrogel injection inhibits post-infarct ventricle remodelling, Eur. J. Heart Fail. 11 (1) (2009) 14–19.
[125] K.L. Fujimoto, Z. Ma, D.M. Nelson, R. Hashizume, J. Guan, K. Tobita, W. R. Wagner, Synthesis, characterization and therapeutic efficacy of a biodegradable, thermoresponsive hydrogel designed for application in chronic infarcted myocardium, Biomaterials 30 (26) (2009) 4357–4368.
[126] J.C. Chachques, O. Jegaden, T. Mesana, Y. Glock, P.A. Grandjean, A.F. Carpentier, Cardiac bioassist: results of the French multicenter cardiomyoplasty study, Asian Cardiovasc. Thorac. Ann. 17 (6) (2009) 573–580.
[127] J.M. Power, J. Raman, A. Dornom, S.J. Farish, L.M. Burrell, A.M. Tonkin, B. Buxton, C.A. Alferness, Passive ventricular constraint amends the course of heart failure: a study in an ovine model of dilated cardiomyopathy, Cardiovasc. Res. 44 (3) (1999) 549–555.
[128] J.A. Magovern, Experimental and clinical studies with the paracor cardiac restraint device, Semin. Thorac. Cardiovasc. Surg. 17 (4) (2005) 364–368.
[129] H.N. Sabbah, Effects of Cardiac Support Device on reverse remodeling: molecular, biochemical, and structural mechanisms, J. Card. Fail. 10 (6) (2004) S207–S214.
[130] S. Chitsaz, J.F. Wenk, L. Ge, A. Wisneski, A. Mookhoek, M.B. Ratcliffe, J. M. Guccione, E.E. Tseng, Material properties of CorCap passive cardiac support device, Ann. Thorac. Surg. 95 (1) (2013) 148–154.
[131] J.M. Power, J. Raman, M.J. Byrne, C.A. Alferness, Efficacy of the Acorn cardiac support device in animals with heart failure secondary to high rate pacing, Heart Fail. Rev. 10 (2) (2005) 117–123.
[132] A.S. Blom, R. Mukherjee, J.J. Pilla, A.S. Lowry, W.M. Yarbrough, J.T. Mingoia, J. W. Hendrick, R.E. Stroud, J.E. McLean, J. Affuso, R.C. Gorman, J.H. Gorman, M. A. Acker, F.G. Spinale, Cardiac support device modifies left ventricular geometry and myocardial structure after myocardial infarction, Circulation 112 (9) (2005) 1274–1283.
[133] G. Speziale, G. Nasso, F. Piancone, K. Generali, C. Paterno, A. Miccoli, F. Fiore, A. Del Prete, G. Del Prete, V. Lopriore, F. Spirito, P. Caldarola, D. Paparella, F. Massari, L. Tavazzi, One-year results after implantation of the CorCap for dilated cardiomyopathy and heart failure, Ann. Thorac. Surg. 91 (5) (2011) 1356–1362.
[134] M.A. Acker, M. Jessup, S.F. Bolling, J. Oh, R.C. Starling, D.L. Mann, H.N. Sabbah, R. Shemin, J. Kirklin, S.H. Kubo, Mitral valve repair in heart failure: five-year follow-up from the mitral valve replacement stratum of the Acorn randomized trial, J. Thorac. Cardiovasc. Surg. 142 (3) (2011) 569–574, e561.
[135] M. Schweiger, A. Stepanenko, E. Potapov, T. Drews, R. Hetzer, T. Krabatsch, Successful implantation of a left ventricular assist device after treatment with the paracor HeartNet, Am. Soc. Artif. Intern. Organs J. 56 (5) (2010).
[136] C.T. Klodell, J.M. Aranda, D.C. McGiffin, B.K. Rayburn, B. Sun, W.T. Abraham, W. E. Pae, J.P. Boehmer, H. Klein, C. Huth, Worldwide surgical experience with the Paracor HeartNet cardiac restraint device, J. Thorac. Cardiovasc. Surg. 135 (1) (2008) 188–195.
[137] A. Rane Aboli, L. Christman Karen, Biomaterials for the treatment of myocardial infarction, J. Am. Coll. Cardiol. 58 (25) (2011) 2615–2629.
[138] V. Serpooshan, M. Zhao, S.A. Metzler, K. Wei, P.B. Shah, A. Wang, M. Mahmoudi, A.V. Malkovskiy, J. Rajadas, M.J. Butte, D. Bernstein, P. Ruiz-Lozano, The effect of bioengineered acellular collagen patch on cardiac remodeling and ventricular function post myocardial infarction, Biomaterials 34 (36) (2013) 9048–9055.
[139] A. Callegari, S. Bollini, L. Iop, A. Chiavegato, G. Torregrossa, M. Pozzobon, G. Gerosa, P. De Coppi, N. Elvassore, S. Sartore, Neovascularization induced by porous collagen scaffold implanted on intact and cryoinjured rat hearts, Biomaterials 28 (36) (2007) 5449–5461.
[140] L. Fujimoto Kazuro, K. Tobita, W.D. Merryman, J. Guan, N. Momoi, B. Stolz Donna, S. Sacks Michael, B. Keller Bradley, R. Wagner William, An elastic, biodegradable cardiac patch induces contractile smooth muscle and improves cardiac remodeling and function in subacute myocardial infarction, J. Am. Coll. Cardiol. 49 (23) (2007) 2292–2300.
[141] R. Hashizume, K.L. Fujimoto, Y. Hong, J. Guan, C. Toma, K. Tobita, W.R. Wagner, Biodegradable elastic patch plasty ameliorates left ventricular adverse remodeling after ischemia–reperfusion injury: a preclinical study of a porous polyurethane material in a porcine model, J. Thorac. Cardiovasc. Surg. 146 (2) (2013) 391–399, e391.
[142] M. Kitahara, S. Miyagawa, S. Fukushima, A. Saito, A. Shintani, T. Akita, Y. Sawa, Biodegradable vs nonbiodegradable cardiac support device for treating ischemic cardiomyopathy in a canine heart, Semin. Thorac. Cardiovasc. Surg. 29 (1) (2017) 51–61.
[143] O. Domengé, H. Ragot, R. Deloux, A. Crépet, G. Revet, S.E. Boitard, A. Simon, N. Mougenot, L. David, T. Delair, A. Montembault, O. Agbulut, Efficacy of epicardial implantation of acellular chitosan hydrogels in ischemic and nonischemic heart failure: impact of the acetylation degree of chitosan, Acta Biomater. (2020).
[144] A. Fiamingo, A. Montembault, S.-E. Boitard, H. Naemetalla, O. Agbulut, T. Delair, S.P. Campana-Filho, P. Menasché, L. David, Chitosan hydrogels for the regeneration of infarcted myocardium: preparation, physicochemical characterization, and biological evaluation, Biomacromolecules 17 (5) (2016) 1662–1672.
[145] X. Lin, Y. Liu, A. Bai, H. Cai, Y. Bai, W. Jiang, H. Yang, X. Wang, L. Yang, N. Sun, H. Gao, A viscoelastic adhesive epicardial patch for treating myocardial infarction, Nature Biomedical Engineering 3 (8) (2019) 632–643.
[146] A.D. Vilaeti, K. Dimos, E.S. Lampri, P. Mantzouratou, N. Tsitou, I. Mourouzis, D. L. Oikonomidis, A. Papalois, C. Pantos, V. Malamou-Mitsi, S. Agathopoulos, T. M. Kolettis, Short-term ventricular restraint attenuates post-infarction remodeling in rats, Int. J. Cardiol. 165 (2) (2013) 278–284.
[147] J. Li, D.J. Mooney, Designing hydrogels for controlled drug delivery, Nature reviews. Materials 1 (12) (2016) 16071.
[148] G.M. Fomovsky, J.R. Macadangdang, G. Ailawadi, J.W. Holmes, Model-based design of mechanical therapies for myocardial infarction, J Cardiovasc Transl Res 4 (1) (2011) 82–91.
[149] A.C. Estrada, K. Yoshida, S.A. Clarke, J.W. Holmes, Longitudinal reinforcement of acute myocardial infarcts improves function by transmurally redistributing stretch and stress, J. Biomech. Eng. 142 (2) (2019).
[150] A.P. Voorhees, H.-C. Han, A model to determine the effect of collagen fiber alignment on heart function post myocardial infarction, Theor. Biol. Med. Model. 11 (2014), 6-6.
[151] G.M. Fomovsky, S.A. Clark, K.M. Parker, G. Ailawadi, J.W. Holmes, Anisotropic reinforcement of acute anteroapical infarcts improves pump function, Circ Heart Fail 5 (4) (2012) 515–522.
[152] P.A. Chaudhry, T. Mishima, V.G. Sharov, J. Hawkins, C. Alferness, G. Paone, H. N. Sabbah, Passive epicardial containment prevents ventricular remodeling in heart failure, Ann. Thorac. Surg. 70 (4) (2000) 1275–1280.
[153] L. Gepstein, Derivation and potential applications of human embryonic stem cells, Circ. Res. 91 (10) (2002) 866–876.
[154] O. Bergmann, R.D. Bhardwaj, S. Bernard, S. Zdunek, F. Barnabé-Heider, S. Walsh, J. Zupicich, K. Alkass, B.A. Buchholz, H. Druid, S. Jovinge, J. Frisén, Evidence for cardiomyocyte renewal in humans, Science 324 (5923) (2009) 98.
[155] O. Bergmann, S. Zdunek, A. Felker, M. Salehpour, K. Alkass, S. Bernard, Staffan L. Sjostrom, M. Szewczykowska, T. Jackowska, C. dos Remedios, T. Malm, M. Andrä, R. Jashari, Jens R. Nyengaard, G. Possnert, S. Jovinge, H. Druid, J. Frisén, Dynamics of cell generation and turnover in the human heart, Cell 161 (7) (2015) 1566–1575.
[156] T. Eschenhagen, R. Bolli, T. Braun, L.J. Field, B.K. Fleischmann, J. Frisén, M. Giacca, J.M. Hare, S. Houser, R.T. Lee, E. Marbán, J.F. Martin, J.D. Molkentin, C.E. Murry, P.R. Riley, P. Ruiz-Lozano, H.A. Sadek, M.A. Sussman, J.A. Hill, Cardiomyocyte regeneration: a consensus statement, Circulation 136 (7) (2017) 680–686.
[157] K. Lietz, W. Long James, G. Kfoury Abdallah, S. Slaughter Mark, A. Silver Marc, A. Milano Carmelo, G. Rogers Joseph, Y. Naka, D. Mancini, W. Miller Leslie, Outcomes of left ventricular assist device implantation as destination therapy in the post-REMATCH era, Circulation 116 (5) (2007) 497–505.
[158] I.T. Center, in: Interagency Registry for Mechanically Assisted Circulatory Support: Quarely Statistical Report 2017 Q3, 2017.
[159] Y. Vaidya, S. Riaz, A.S. Dhamoon, Left ventricular assist devices (LVAD), in: *StatPearls*. Treasure Island (FL), 2020.
[160] A. Tsiouris, G. Paone, H.W. Nemeh, J. Borgi, C.T. Williams, D.E. Lanfear, J. A. Morgan, Short and long term outcomes of 200 patients supported by continuous-flow left ventricular assist devices, World J. Cardiol. 7 (11) (2015) 792–800.
[161] G. Torregrossa, M. Morshuis, R. Varghese, L. Hosseinian, V. Vida, V. Tarzia, A. Loforte, D. Duveau, F. Arabia, P. Leprince, V. Kasirajan, F. Beyersdorf, F. Musumeci, R. Hetzer, T. Krabatsch, J. Gummert, J. Copeland, G. Gerosa, Results with SynCardia total artificial heart beyond 1 year, Am. Soc. Artif. Intern. Organs J. 60 (6) (2014) 626–634.
[162] C.J. Payne, I. Wamala, C. Abah, T. Thalhofer, M. Saeed, D. Bautista-Salinas, M. A. Horvath, N.V. Vasilyev, E.T. Roche, F.A. Pigula, C.J. Walsh, An implantable extracardiac soft robotic device for the failing heart: mechanical coupling and synchronization, Soft Robot. 4 (3) (2017) 241–250.
[163] C.J. Payne, I. Wamala, D. Bautista-Salinas, M. Saeed, D. Van Story, T. Thalhofer, M.A. Horvath, C. Abah, P.J. del Nido, C.J. Walsh, N.V. Vasilyev, Soft robotic ventricular assist device with septal bracing for therapy of heart failure, Science Robotics 2 (12) (2017), eaan6736.
[164] B.C. Mac Murray, C.C. Futran, J. Lee, K.W. O'Brien, A.A. Amiri Moghadam, B. Mosadegh, M.N. Silberstein, J.K. Min, R.F. Shepherd, Compliant buckled foam actuators and application in patient-specific direct cardiac compression, Soft Robot. 5 (1) (2018) 99–108.
[165] J.C. Chachques, J.C. Trainini, N. Lago, M. Cortes-Morichetti, O. Schussler, A. Carpentier, Myocardial assistance by grafting a new bioartificial upgraded myocardium (MAGNUM trial): clinical feasibility study, Ann. Thorac. Surg. 85 (3) (2008) 901–908.
[166] M. Domenech, L. Polo-Corrales, J.E. Ramirez-Vick, D.O. Freytes, Tissue engineering strategies for myocardial regeneration: acellular versus cellular scaffolds? *Tissue engineering*, Part B, Reviews 22 (6) (2016) 438–458.
[167] E. Karbassi, A. Fenix, S. Marchiano, N. Muraoka, K. Nakamura, X. Yang, C. E. Murry, Cardiomyocyte maturation: advances in knowledge and implications for regenerative medicine, Nat. Rev. Cardiol. (2020).
[168] Y. Jiang, P. Park, S.-M. Hong, K. Ban, Maturation of cardiomyocytes derived from human pluripotent stem cells: current strategies and limitations, Mol. Cell. 41 (7) (2018) 613–621.
[169] X. Yang, L. Pabon, C.E. Murry, Engineering adolescence: maturation of human pluripotent stem cell-derived cardiomyocytes, Circ. Res. 114 (3) (2014) 511–523.
[170] C.C. Veerman, G. Kosmidis, C.L. Mummery, S. Casini, A.O. Verkerk, M. Bellin, Immaturity of human stem-cell-derived cardiomyocytes in culture: fatal flaw or soluble problem? Stem Cell. Dev. 24 (9) (2015) 1035–1052.
[171] S. Kannan, M. Farid, B.L. Lin, M. Miyamoto, C. Kwon, Transcriptomic Entropy Quantifies Cardiomyocyte Maturation at Single Cell Level, 2020.

[172] J.P. Guyette, J.M. Charest, R.W. Mills, B.J. Jank, P.T. Moser, S.E. Gilpin, J. R. Gershlak, T. Okamoto, G. Gonzalez, D.J. Milan, G.R. Gaudette, H.C. Ott, Bioengineering human myocardium on native extracellular matrix, Circ. Res. 118 (1) (2016) 56–72.
[173] L. Iop, E. Dal Sasso, R. Menabò, F. Di Lisa, G. Gerosa, The rapidly evolving concept of whole heart engineering, Stem Cell. Int. (2017). *2017*, 8920940-8920940.
[174] D. Bejleri, M.E. Davis, Decellularized extracellular matrix materials for cardiac repair and regeneration, Advanced Healthcare Materials 8 (5) (2019) 1801217.
[175] J. Schwan, A.T. Kwaczala, T.J. Ryan, O. Bartulos, Y. Ren, L.R. Sewanan, A. H. Morris, D.L. Jacoby, Y. Qyang, S.G. Campbell, Anisotropic engineered heart tissue made from laser-cut decellularized myocardium, Sci. Rep. 6 (1) (2016) 32068.
[176] A. Blazeski, G.M. Kostecki, L. Tung, Engineered heart slices for electrophysiological and contractile studies, Biomaterials 55 (2015) 119–128.
[177] J. Musilkova, E. Filova, J. Pala, R. Matejka, D. Hadraba, D. Vondrasek, O. Kaplan, T. Riedel, E. Brynda, J. Kucerova, M. Konarik, F. Lopot, P. Jan, L. Bacakova, Human decellularized and crosslinked pericardium coated with bioactive molecular assemblies, Biomed. Mater. 15 (1) (2019), 015008.
[178] I. Perea-Gil, C. Gálvez-Montón, C. Prat-Vidal, I. Jorba, C. Segú-Vergés, S. Roura, C. Soler-Botija, O. Iborra-Egea, E. Revuelta-López, M.A. Fernández, R. Farré, D. Navajas, A. Bayes-Genis, Head-to-head comparison of two engineered cardiac grafts for myocardial repair: from scaffold characterization to pre-clinical testing, Sci. Rep. 8 (1) (2018) 6708.
[179] E.d.O. Lima, A.C. Ferrasi, A. Kaasi, Decellularization of human pericardium with potential application in regenerative medicine, Arq. Bras. Cardiol. 113 (1) (2019) 18–19.
[180] E.R. Robbins, G.D. Pins, M.A. Laflamme, G.R. Gaudette, Creation of a contractile biomaterial from a decellularized spinach leaf without ECM protein coating: an in vitro study, J. Biomed. Mater. Res. (2020) n/a(n/a).
[181] J.R. Gershlak, S. Hernandez, G. Fontana, L.R. Perreault, K.J. Hansen, S.A. Larson, B.Y. Binder, D.M. Dolivo, T. Yang, T. Dominko, M.W. Rolle, P.J. Weathers, F. Medina-Bolivar, C.L. Cramer, W.L. Murphy, G.R. Gaudette, Crossing kingdoms: using decellularized plants as perfusable tissue engineering scaffolds, Biomaterials 125 (2017) 13–22.
[182] W.L. Stoppel, D. Hu, I.J. Domian, D.L. Kaplan, L.D. Black 3rd, Anisotropic silk biomaterials containing cardiac extracellular matrix for cardiac tissue engineering, Biomed. Mater. 10 (3) (2015), 034105.
[183] M.M. Smoak, A. Han, E. Watson, A. Kishan, K.J. Grande-Allen, E. Cosgriff-Hernandez, A.G. Mikos, Fabrication and characterization of electrospun decellularized muscle-derived scaffolds, Tissue Eng. C Methods 25 (5) (2019) 276–287.
[184] W. Bian, C.P. Jackman, N. Bursac, Controlling the structural and functional anisotropy of engineered cardiac tissues, Biofabrication 6 (2) (2014), 024109-24109.
[185] L.L. Chiu, K. Janic, M. Radisic, Engineering of oriented myocardium on three-dimensional micropatterned collagen-chitosan hydrogel, Int. J. Artif. Organs 35 (4) (2012) 237–250.
[186] F. Munarin, N.J. Kaiser, T.Y. Kim, B.-R. Choi, K.L.K. Coulombe, Laser-etched designs for molding hydrogel-based engineered tissues, Tissue Eng. C Methods 23 (5) (2017) 311–321.
[187] J.I. Luna, J. Ciriza, M.E. Garcia-Ojeda, M. Kong, A. Herren, D.K. Lieu, R.A. Li, C. C. Fowlkes, M. Khine, K.E. McCloskey, Multiscale biomimetic topography for the alignment of neonatal and embryonic stem cell-derived heart cells, Tissue Eng. C Methods 17 (5) (2011) 579–588.
[188] G.C. Engelmayr, M. Cheng, C.J. Bettinger, J.T. Borenstein, R. Langer, L.E. Freed, Accordion-like honeycombs for tissue engineering of cardiac anisotropy, Nat. Mater. 7 (12) (2008) 1003–1010.
[189] M. Mao, J. He, Z. Li, K. Han, D. Li, Multi-directional cellular alignment in 3D guided by electrohydrodynamically-printed microlattices, Acta Biomater. 101 (2020) 141–151.
[190] M.W. Toepke, D.J. Beebe, PDMS absorption of small molecules and consequences in microfluidic applications, Lab Chip 6 (12) (2006) 1484–1486.
[191] V. Tandon, B. Zhang, M. Radisic, S.K. Murthy, Generation of tissue constructs for cardiovascular regenerative medicine: from cell procurement to scaffold design, Biotechnol. Adv. 31 (5) (2013) 722–735.
[192] I.M. El-Sherbiny, M.H. Yacoub, Hydrogel scaffolds for tissue engineering: progress and challenges, Global Cardiology Science and Practice 2013 (3) (2013).
[193] A.C.B. Allen, E. Barone, N. Momtahan, C.O. Crosby, C. Tu, W. Deng, K. Polansky, J. Zoldan, Temporal impact of substrate anisotropy on differentiating cardiomyocyte alignment and functionality, Tissue Eng. 25 (19–20) (2019) 1426–1437.
[194] M. Dn, S. A, D. Mavrilas, Tuning fiber alignment to achieve mechanical anisotropy on polymeric electrospun scaffolds for cardiovascular tissue engineering, J. Mater. Sci. Eng. 7 (4) (2018).
[195] N. Adadi, M. Yadid, I. Gal, M. Asulin, R. Feiner, R. Edri, T. Dvir, Electrospun fibrous PVDF-TrFe scaffolds for cardiac tissue engineering, differentiation, and maturation, Advanced Materials Technologies 5 (3) (2020) 1900820.
[196] S. Fleischer, A. Shapira, O. Regev, N. Nseir, E. Zussman, T. Dvir, Albumin fiber scaffolds for engineering functional cardiac tissues, Biotechnol. Bioeng. 111 (6) (2014) 1246–1257.
[197] L.A. MacQueen, S.P. Sheehy, C.O. Chantre, J.F. Zimmerman, F.S. Pasqualini, X. Liu, J.A. Goss, P.H. Campbell, G.M. Gonzalez, S.J. Park, A.K. Capulli, J. P. Ferrier, T.F. Kosar, L. Mahadevan, W.T. Pu, K.K. Parker, A tissue-engineered scale model of the heart ventricle, Nat Biomed Eng 2 (12) (2018) 930–941.
[198] Y. Orlova, N. Magome, L. Liu, Y. Chen, K. Agladze, Electrospun nanofibers as a tool for architecture control in engineered cardiac tissue, Biomaterials 32 (24) (2011) 5615–5624.
[199] X. Zong, H. Bien, C.-Y. Chung, L. Yin, D. Fang, B.S. Hsiao, B. Chu, E. Entcheva, Electrospun fine-textured scaffolds for heart tissue constructs, Biomaterials 26 (26) (2005) 5330–5338.
[200] M. Wanjare, L. Hou, K.H. Nakayama, J.J. Kim, N.P. Mezak, O.J. Abilez, E. Tzatzalos, J.C. Wu, N.F. Huang, Anisotropic microfibrous scaffolds enhance the organization and function of cardiomyocytes derived from induced pluripotent stem cells, Biomater Sci 5 (8) (2017) 1567–1578.
[201] L.D. Black, J.D. Meyers, J.S. Weinbaum, Y.A. Shvelidze, R.T. Tranquillo, Cell-induced alignment augments twitch force in fibrin gel–based engineered myocardium via gap junction modification, Tissue Eng. 15 (10) (2009) 3099–3108.
[202] M.O. Chrobak, K.J. Hansen, J.R. Gershlak, M. Vratsanos, M. Kanellias, G. R. Gaudette, G.D. Pins, Design of a fibrin microthread-based composite layer for use in a cardiac patch, ACS Biomater. Sci. Eng. 3 (7) (2017) 1394–1403.
[203] H. Cui, C. Liu, T. Esworthy, Y. Huang, Z.-x. Yu, X. Zhou, H. San, S.-j. Lee, S. Y. Hann, M. Boehm, M. Mohiuddin, J.P. Fisher, L.G. Zhang, 4D physiologically adaptable cardiac patch: a 4-month in vivo study for the treatment of myocardial infarction, Science Advances 6 (26) (2020), eabb5067.
[204] T. Nakane, H. Masumoto, J.P. Tinney, F. Yuan, W.J. Kowalski, F. Ye, A.J. LeBlanc, R. Sakata, J.K. Yamashita, B.B. Keller, Impact of cell composition and geometry on human induced pluripotent stem cells-derived engineered cardiac tissue, Sci. Rep. 7 (1) (2017) 45641.
[205] D.G. Simpson, W.W. Sharp, T.K. Borg, R.L. Price, A.M. Samarel, L. Terracio, Mechanical regulation of cardiac myofibrillar structure, Ann. N. Y. Acad. Sci. 752 (1995) 131–140.
[206] J.E.T. van Wamel, C. Ruwhof, E.J.M. van der Valk-Kokshoorn, P.I. Schrier, A. van der Laarse, Rapid gene transcription induced by stretch in cardiac myocytes and fibroblasts and their paracrine influence on stationary myocytes and fibroblasts, Pflügers Archiv 439 (6) (2000) 781–788.
[207] C. Fink, S. Ergün, D. Kralisch, U. Remmers, J. Weil, T. Eschenhagen, Chronic stretch of engineered heart tissue induces hypertrophy and functional improvement, Faseb. J. 14 (5) (2000) 669–679.
[208] A. Salameh, A. Wustmann, S. Karl, K. Blanke, D. Apel, D. Rojas-Gomez, H. Franke, W. Mohr Friedrich, J. Janousek, S. Dhein, Cyclic mechanical stretch induces cardiomyocyte orientation and polarization of the gap junction protein Connexin43, Circ. Res. 106 (10) (2010) 1592–1602.
[209] L. Tulloch Nathaniel, V. Muskheli, V. Razumova Maria, F.S. Korte, M. Regnier, D. Hauch Kip, L. Pabon, H. Reinecke, E. Murry Charles, Growth of engineered human myocardium with mechanical loading and vascular coculture, Circ. Res. 109 (1) (2011) 47–59.
[210] W.-H. Zimmermann, I. Melnychenko, G. Wasmeier, M. Didié, H. Naito, U. Nixdorff, A. Hess, L. Budinsky, K. Brune, B. Michaelis, S. Dhein, A. Schwoerer, H. Ehmke, T. Eschenhagen, Engineered heart tissue grafts improve systolic and diastolic function in infarcted rat hearts, Nat. Med. 12 (4) (2006) 452–458.
[211] M. Shachar, N. Benishti, S. Cohen, Effects of mechanical stimulation induced by compression and medium perfusion on cardiac tissue engineering, Biotechnol. Prog. 28 (6) (2012) 1551–1559.
[212] P. Akhyari, W.M. Fedak Paul, D. Weisel Richard, J. Lee Tsu-Yee, S. Verma, A. G. Mickle Donald, R.-K. Li, Mechanical stretch regimen enhances the formation of bioengineered autologous cardiac muscle grafts, Circulation 106 (12_suppl_1) (2002). I-137-I-142.
[213] W.H. Zimmermann, K. Schneiderbanger, P. Schubert, M. Didié, F. Münzel, J. F. Heubach, S. Kostin, W.L. Neuhuber, T. Eschenhagen, Tissue engineering of a differentiated cardiac muscle construct, Circ. Res. 90 (2) (2002) 223–230.
[214] H. Atcha, C.T. Davis, N.R. Sullivan, T.D. Smith, S. Anis, W.Z. Dahbour, Z. R. Robinson, A. Grosberg, W.F. Liu, A low-cost mechanical stretching device for uniaxial strain of cells: a platform for pedagogy in mechanobiology, J. Biomech. Eng. 140 (8) (2018).
[215] M. Govoni, C. Muscari, C. Guarnieri, E. Giordano, Mechanostimulation protocols for cardiac tissue engineering, BioMed Res. Int. 2013 (2013) 918640.
[216] K.Y. Morgan, L.D. Black 3rd, Mimicking isovolumic contraction with combined electromechanical stimulation improves the development of engineered cardiac constructs, Tissue Eng. 20 (11–12) (2014) 1654–1667.
[217] A.F. Godier-Furnémont, M. Tiburcy, E. Wagner, M. Dewenter, S. Lämmle, A. El-Armouche, S.E. Lehnart, G. Vunjak-Novakovic, W.H. Zimmermann, Physiologic force-frequency response in engineered heart muscle by electromechanical stimulation, Biomaterials 60 (2015) 82–91.
[218] A. Au - Llucià-Valldeperas, R. Au - Bragós, A. Au - Bayés-Genís, Simultaneous electrical and mechanical stimulation to enhance cells' cardiomyogenic potential, JoVE 143 (2019), e58934.
[219] A. Llucià-Valldeperas, C. Soler-Botija, C. Gálvez-Montón, S. Roura, C. Prat-Vidal, I. Perea-Gil, B. Sanchez, R. Bragos, G. Vunjak-Novakovic, A. Bayes-Genis, Electromechanical conditioning of adult progenitor cells improves recovery of cardiac function after myocardial infarction, Stem Cells Transl Med 6 (3) (2017) 970–981.
[220] H.T. Heidi Au, B. Cui, Z.E. Chu, T. Veres, M. Radisic, Cell culture chips for simultaneous application of topographical and electrical cues enhance phenotype of cardiomyocytes, Lab Chip 9 (4) (2009) 564–575.
[221] H.T.H. Au, I. Cheng, M.F. Chowdhury, M. Radisic, Interactive effects of surface topography and pulsatile electrical field stimulation on orientation and elongation of fibroblasts and cardiomyocytes, Biomaterials 28 (29) (2007) 4277–4293.

[222] P. Anversa, A. Loud, F. Giacomelli, J. Wiener, Absolute morphometric study of myocardial hypertrophy in experimental hypertension. II. Ultrastructure of myocytes and interstitium, Laboratory investigation; a journal of technical methods and pathology 38 (5) (1978) 597–609.
[223] O. Bergmann, S. Zdunek, A. Felker, M. Salehpour, K. Alkass, S. Bernard, S. L. Sjostrom, M. Szewczykowska, T. Jackowska, C. Dos Remedios, Dynamics of cell generation and turnover in the human heart, Cell 161 (7) (2015) 1566–1575.
[224] D.A. Skelly, G.T. Squiers, M.A. McLellan, M.T. Bolisetty, P. Robson, N. A. Rosenthal, A.R. Pinto, Single-cell transcriptional profiling reveals cellular diversity and intercommunication in the mouse heart, Cell Rep. 22 (3) (2018) 600–610.
[225] H. Sekine, T. Shimizu, K. Hobo, S. Sekiya, J. Yang, M. Yamato, H. Kurosawa, E. Kobayashi, T. Okano, Endothelial cell coculture within tissue-engineered cardiomyocyte sheets enhances neovascularization and improves cardiac function of ischemic hearts, Circulation 118 (14_suppl_1) (2008) S145–S152.
[226] K.L. Kreutziger, V. Muskheli, P. Johnson, K. Braun, T.N. Wight, C.E. Murry, Developing vasculature and stroma in engineered human myocardium, Tissue Eng. 17 (9–10) (2010) 1219–1228.
[227] K.R. Stevens, K.L. Kreutziger, S.K. Dupras, F.S. Korte, M. Regnier, V. Muskheli, M. B. Nourse, K. Bendixen, H. Reinecke, C.E. Murry, Physiological function and transplantation of scaffold-free and vascularized human cardiac muscle tissue, Proc. Natl. Acad. Sci. Unit. States Am. 106 (39) (2009) 16568.
[228] J.S. Wendel, L. Ye, R. Tao, J. Zhang, J. Zhang, T.J. Kamp, R.T. Tranquillo, Functional effects of a tissue-engineered cardiac patch from human induced pluripotent stem cell-derived cardiomyocytes in a rat infarct model, STEM CELLS Translational Medicine 4 (11) (2015) 1324–1332.
[229] T.J. Owen, S.E. Harding, Multi-cellularity in cardiac tissue engineering, how close are we to native heart tissue? J. Muscle Res. Cell Motil. 40 (2) (2019) 151–157.
[230] B. Liau, C.P. Jackman, Y. Li, N. Bursac, Developmental stage-dependent effects of cardiac fibroblasts on function of stem cell-derived engineered cardiac tissues, Sci. Rep. 7 (2017) 42290.
[231] G. Kensah, A. Roa Lara, J. Dahlmann, R. Zweigerdt, K. Schwanke, J. Hegermann, D. Skvorc, A. Gawol, A. Azizian, S. Wagner, L.S. Maier, A. Krause, G. Dräger, M. Ochs, A. Haverich, I. Gruh, U. Martin, Murine and human pluripotent stem cell-derived cardiac bodies form contractile myocardial tissue in vitro, Eur. Heart J. 34 (15) (2013) 1134–1146.
[232] C.E. Rupert, T.Y. Kim, B.-R. Choi, K.L.K. Coulombe, Human cardiac fibroblast number and activation state modulate electromechanical function of hiPSC-cardiomyocytes in engineered myocardium, Stem Cell. Int. 2020 (2020), 9363809.
[233] P. Beauchamp, C.B. Jackson, L.C. Ozhathil, I. Agarkova, C.L. Galindo, D. B. Sawyer, T.M. Suter, C. Zuppinger, 3D Co-culture of hiPSC-derived cardiomyocytes with cardiac fibroblasts improves tissue-like features of cardiac spheroids, Frontiers in molecular biosciences 7 (2020), 14-14.
[234] A. Weeke-Klimp, N.A.M. Bax, A.R. Bellu, E.M. Winter, J. Vrolijk, J. Plantinga, S. Maas, M. Brinker, E.A.F. Mahtab, A.C. Gittenberger-de Groot, M.J.A. van Luyn, M.C. Harmsen, H. Lie-Venema, Epicardium-derived cells enhance proliferation, cellular maturation and alignment of cardiomyocytes, J. Mol. Cell. Cardiol. 49 (4) (2010) 606–616.
[235] I. Stuckmann, S. Evans, A.B. Lassar, Erythropoietin and retinoic acid, secreted from the epicardium, are required for cardiac myocyte proliferation, Dev. Biol. 255 (2) (2003) 334–349.
[236] H. Eid, D.M. Larson, J.P. Springhorn, M.A. Attawia, R.C. Nayak, T.W. Smith, R. A. Kelly, Role of epicardial mesothelial cells in the modification of phenotype and function of adult rat ventricular myocytes in primary coculture, Circ. Res. 71 (1) (1992) 40–50.
[237] J. Bargehr, L.P. Ong, M. Colzani, H. Davaapil, P. Hofsteen, S. Bhandari, L. Gambardella, N. Le Novère, D. Iyer, F. Sampaziotis, F. Weinberger, A. Bertero, A. Leonard, W.G. Bernard, A. Martinson, N. Figg, M. Regnier, M.R. Bennett, C. E. Murry, S. Sinha, Epicardial cells derived from human embryonic stem cells augment cardiomyocyte-driven heart regeneration, Nat. Biotechnol. 37 (8) (2019) 895–906.
[238] M.N. Monroe, R.C. Nikonowicz, K.J. Grande-Allen, Heterogeneous multi-laminar tissue constructs as a platform to evaluate aortic valve matrix-dependent pathogenicity, Acta Biomater. 97 (2019) 420–427.
[239] K. Yuan Ye, K.E. Sullivan, L.D. Black, Encapsulation of cardiomyocytes in a fibrin hydrogel for cardiac tissue engineering, JoVE 55 (2011).
[240] J.A. Schaefer, R.T. Tranquillo, Tissue contraction force microscopy for optimization of engineered cardiac tissue, Tissue Eng. C Methods 22 (1) (2016) 76–83.
[241] S. Roura, C. Soler-Botija, J.R. Bagó, A. Llucià-Valldeperas, M.A. Férnandez, C. Gálvez-Montón, C. Prat-Vidal, I. Perea-Gil, J. Blanco, A. Bayes-Genis, Postinfarction functional recovery driven by a three-dimensional engineered fibrin patch composed of human umbilical cord blood-derived mesenchymal stem cells, STEM CELLS Translational Medicine 4 (8) (2015) 956–966.
[242] C.E. Rupert, K.L.K. Coulombe, IGF1 and NRG1 enhance proliferation, metabolic maturity, and the force-frequency response in hESC-derived engineered cardiac tissues, Stem Cell. Int. (2017) 7648409, 2017.
[243] T. Eschenhagen, M. Didié, F. Münzel, P. Schubert, K. Schneiderbanger, W. H. Zimmermann, 3D engineered heart tissue for replacement therapy, Basic Res. Cardiol. 97 (Suppl 1) (2002) I146–I152.
[244] N.J. Kaiser, R.J. Kant, A.J. Minor, K.L.K. Coulombe, Optimizing blended collagen-fibrin hydrogels for cardiac tissue engineering with human iPSC-derived cardiomyocytes, ACS Biomater. Sci. Eng. 5 (2) (2019) 887–899.
[245] N. Milani-Nejad, P.M.L. Janssen, Small and large animal models in cardiac contraction research: advantages and disadvantages, Pharmacol. Ther. 141 (3) (2014) 235–249.
[246] K. Nakao, W. Minobe, R. Roden, M.R. Bristow, L.A. Leinwand, Myosin heavy chain gene expression in human heart failure, J. Clin. Invest. 100 (9) (1997) 2362–2370.
[247] S. Miyata, W. Minobe, M.R. Bristow, L.A. Leinwand, Myosin heavy chain isoform expression in the failing and nonfailing human heart, Circ. Res. 86 (4) (2000) 386–390.
[248] P.J. Reiser, M.A. Portman, X.H. Ning, C. Schomisch Moravec, Human cardiac myosin heavy chain isoforms in fetal and failing adult atria and ventricles, Am. J. Physiol. Heart Circ. Physiol. 280 (4) (2001) H1814–H1820.
[249] D.D. Lemon, P.J. Papst, K. Joly, C.F. Plato, T.A. McKinsey, A high-performance liquid chromatography assay for quantification of cardiac myosin heavy chain isoform protein expression, Anal. Biochem. 408 (1) (2011) 132–135.
[250] P. Camacho, H. Fan, Z. Liu, J.-Q. He, Large mammalian animal models of heart disease, Journal of cardiovascular development and disease 3 (4) (2016) 30.
[251] V. Tyberg John, S. Forrester James, H.L. Wyatt, J. Goldner Steven, W. Parmley William, H.J.C. Swan, An analysis of segmental ischemic dysfunction utilizing the pressure-length loop, Circulation 49 (4) (1974) 748–754.
[252] P.M. Tan, K.S. Buchholz, J.H. Omens, A.D. McCulloch, J.J. Saucerman, Predictive model identifies key network regulators of cardiomyocyte mechano-signaling, PLoS Comput. Biol. 13 (11) (2017), e1005854.
[253] R.K. Ghanta, A. Rangaraj, R. Umakanthan, L. Lee, R.G. Laurence, J.A. Fox, R. M. Bolman, L.H. Cohn, F.Y. Chen, Adjustable, physiological ventricular restraint improves left ventricular mechanics and reduces dilatation in an ovine model of chronic heart failure, Circulation 115 (10) (2007) 1201–1210.
[254] L.S. Lee, R.K. Ghanta, S.A. Mokashi, O. Coelho-Filho, R.Y. Kwong, M. Kwon, J. Guan, R. Liao, F.Y. Chen, Optimized ventricular restraint therapy: adjustable restraint is superior to standard restraint in an ovine model of ischemic cardiomyopathy, J. Thorac. Cardiovasc. Surg. 145 (3) (2013) 824–831.
[255] A.B. Stein, S. Tiwari, P. Thomas, G. Hunt, C. Levent, M.F. Stoddard, X.L. Tang, R. Bolli, B. Dawn, Effects of anesthesia on echocardiographic assessment of left ventricular structure and function in rats, Basic Res. Cardiol. 102 (1) (2007) 28–41.
[256] C.A. Cezar, P. Arany, S.A. Vermillion, B.R. Seo, H.H. Vandenburgh, D.J. Mooney, Timed delivery of therapy enhances functional muscle regeneration, Adv Healthc Mater 6 (19) (2017).
[257] W. Whyte, E.T. Roche, C.E. Varela, K. Mendez, S. Islam, H. O'Neill, F. Weafer, R. N. Shirazi, J.C. Weaver, N.V. Vasilyev, P.E. McHugh, B. Murphy, G.P. Duffy, C. J. Walsh, D.J. Mooney, Sustained release of targeted cardiac therapy with a replenishable implanted epicardial reservoir, Nat Biomed Eng 2 (6) (2018) 416–428.
[258] F. Munarin, R.J. Kant, C.E. Rupert, A. Khoo, K.L.K. Coulombe, Engineered human myocardium with local release of angiogenic proteins improves vascularization and cardiac function in injured rat hearts, Biomaterials 251 (2020) 120033.
[259] N. Bloise, I. Rountree, C. Polucha, G. Montagna, L. Visai, K.L.K. Coulombe, F. Munarin, Engineering immunomodulatory biomaterials for regenerating the infarcted myocardium, Frontiers in Bioengineering and Biotechnology 8 (292) (2020).
[260] K. Huang, E.W. Ozpinar, T. Su, J. Tang, D. Shen, L. Qiao, S. Hu, Z. Li, H. Liang, K. Mathews, V. Scharf, D.O. Freytes, K. Cheng, An off-the-shelf artificial cardiac patch improves cardiac repair after myocardial infarction in rats and pigs, Sci. Transl. Med. 12 (538) (2020), eaat9683.
[261] H. Yu, Z. Wang, Cardiomyocyte-derived exosomes: biological functions and potential therapeutic implications, Front. Physiol. 10 (1049) (2019).
[262] K.I. Mentkowski, J.K. Lang, Exosomes engineered to express a cardiomyocyte binding peptide demonstrate improved cardiac retention in vivo, Sci. Rep. 9 (1) (2019) 10041.
[263] M. Hu, G. Guo, Q. Huang, C. Cheng, R. Xu, A. Li, N. Liu, S. Liu, The harsh microenvironment in infarcted heart accelerates transplanted bone marrow mesenchymal stem cells injury: the role of injured cardiomyocytes-derived exosomes, Cell Death Dis. 9 (3) (2018) 357.
[264] R.S. Kellar, B.R. Shepherd, D.F. Larson, G.K. Naughton, S.K. Williams, Cardiac patch constructed from human fibroblasts attenuates reduction in cardiac function after acute infarct, Tissue Eng. 11 (11–12) (2005) 1678–1687.
[265] Q. Xiong, K.L. Hill, Q. Li, P. Suntharalingam, A. Mansoor, X. Wang, M.N. Jameel, P. Zhang, C. Swingen, D.S. Kaufman, J. Zhang, A fibrin patch-based enhanced delivery of human embryonic stem cell-derived vascular cell transplantation in a porcine model of postinfarction left ventricular remodeling, Stem Cell. 29 (2) (2011) 367–375.
[266] Kashiyama, N., Kormos, R. L., Matsumura, Y., D'Amore, A., Miyagawa, S., Sawa, Y., & Wagner, W. R. Adipose-derived stem cell sheet under an elastic patch improves cardiac function in rats after myocardial infarction. J. Thorac. Cardiovasc. Surg..
[267] S. Roura, C. Gálvez-Montón, C. Mirabel, J. Vives, A. Bayes-Genis, Mesenchymal stem cells for cardiac repair: are the actors ready for the clinical scenario? Stem Cell Res. Ther. 8 (1) (2017) 238.
[268] G. Gaudesius, M. Miragoli, S.P. Thomas, S. Rohr, Coupling of cardiac electrical activity over extended distances by fibroblasts of cardiac origin, Circ. Res. 93 (5) (2003) 421–428.
[269] K.A. Gerbin, X. Yang, C.E. Murry, K.L.K. Coulombe, Enhanced electrical integration of engineered human myocardium via intramyocardial versus epicardial delivery in infarcted rat hearts, PloS One 10 (7) (2015), e0131446.
[270] N. Behabtu, C.C. Young, D.E. Tsentalovich, O. Kleinerman, X. Wang, A.W.K. Ma, E.A. Bengio, R.F. ter Waarbeek, J.J. de Jong, R.E. Hoogerwerf, S.B. Fairchild, J.

B. Ferguson, B. Maruyama, J. Kono, Y. Talmon, Y. Cohen, M.J. Otto, M. Pasquali, Strong, light, multifunctional fibers of carbon nanotubes with ultrahigh conductivity, Science 339 (6116) (2013) 182.

[271] D. McCauley Mark, F. Vitale, J.S. Yan, C. Young Colin, B. Greet, M. Orecchioni, S. Perike, A. Elgalad, A. Coco Julia, M. John, A. Taylor Doris, C. Sampaio Luiz, G. Delogu Lucia, M. Razavi, M. Pasquali, In vivo restoration of myocardial conduction with carbon nanotube fibers, Circulation: Arrhythmia and Electrophysiology 12 (8) (2019), e007256.

[272] J. Park, S. Choi, A.H. Janardhan, S.-Y. Lee, S. Raut, J. Soares, K. Shin, S. Yang, C. Lee, K.-W. Kang, H.R. Cho, S.J. Kim, P. Seo, W. Hyun, S. Jung, H.-J. Lee, N. Lee, S.H. Choi, M. Sacks, N. Lu, M.E. Josephson, T. Hyeon, D.-H. Kim, H.J. Hwang, Electromechanical cardioplasty using a wrapped elasto-conductive epicardial mesh, Sci. Transl. Med. 8 (344) (2016) 344ra386.

[273] P. Baei, M. Hosseini, H. Baharvand, S. Pahlavan, Electrically conductive materials for in vitro cardiac microtissue engineering, J. Biomed. Mater. Res. 108 (5) (2020) 1203–1213.